nature communications

Article

https://doi.org/10.1038/s41467-025-58644-2

Colonic epithelial-derived FGF1 drives intestinal stem cell commitment toward goblet cells to suppress inflammatory bowel disease

Received: 11 October 2024

Accepted: 31 March 2025

Published online: 05 April 2025

Check for updates

Qian Lin[1,6], Sudan Zhang[1,6], Jiaren Zhang[1,6], Yi Jin[2,6], Taoli Chen[3], Ruoyu Lin[1], Jiaxuan Lv[1], Wenjing Xu[1], Tianzhen Wu[1], Shenyu Tian[1], Lei Ying[4], Xiaokun Li[1], Zhifeng Huang[1,5] ✉ & Jianlou Niu[1] ✉

Understanding the molecular mechanisms that regulate intestinal epithelial cell (IEC) renewal provides potential targets for inflammatory bowel disease (IBD). Growing evidence has highlighted the importance of epithelial signals in regulating intestinal stem cell (ISC) differentiation. However, it remains unclear which IEC-derived cytokines can precisely regulate ISC commitment toward specific mature cells. Here we systematically analyze all fibroblast growth factors (FGFs) expression and find that colonic FGF1 levels are inversely correlated with the severity of IBD in mouse models and patients. IEC-specific *Fgf1* deletion leads to impaired goblet cell differentiation and exacerbated colitis, while pharmacological administration of recombinant FGF1 (rFGF1) alleviates colitis by enhancing goblet cell differentiation and improving colonic epithelial integrity. Mechanistic studies reveal that rFGF1 directs ISC differentiation toward goblet cells via FGFR2-TCF4-ATOH1 signaling axis. In conclusion, our study identifies an epithelial niche-derived FGF1 that regulates ISC commitment toward goblet cells, shedding light on strategies for treating IBD.

Inflammatory bowel disease (IBD) is a chronic gastrointestinal disease consisting of two subtypes: ulcerative colitis (UC)[1] and Crohn's disease (CD)[2]. IBD is a worldwide spread disease with increasing incidence rate which severely threatens public health[3]. Currently, therapeutic approaches for this disease include 5-aminosalicylic acid (5-ASA), steroids (prednisone, budesonide), immunomodulators and targeted biologic therapies[1,4]. However, they can only alleviate clinical symptoms of IBD. It has been estimated that almost 30% of IBD patients do not respond to current therapies and this proportion is increasing with treatment progresses[5]. Thus, it is urgent to develop novel therapies for the treatment of IBD.

The intestinal epithelial barrier, comprised of secretory lineage (goblet, enteroendocrine and tuft cells) and absorptive enterocytes, differentiates from intestinal stem cells (ISCs) residing at the bottom of crypts, and provides a critical physical and immunological barrier between host and external environment (i.e. luminal contents)[6–8].

[1]State Key Laboratory of Macromolecular Drugs and Large-scale Preparation, School of Pharmaceutical Sciences, Wenzhou Medical University, Wenzhou, Zhejiang 325035, China. [2]Department of Pathology, The First Affiliated Hospital of Wenzhou Medical University, Wenzhou 325035 Zhejiang, China. [3]Department of Pharmacy, The Second Affiliated Hospital of Jiaxing University, Jiaxing 314000 Zhejiang, China. [4]School of Basic Medical Sciences, Wenzhou Medical University, Wenzhou, Zhejiang 325035, China. [5]Translational Medicine Laboratory, The First Affiliated Hospital of Wenzhou Medical University, Wenzhou, Zhejiang 325035, China. [6]These authors contributed equally: Qian Lin, Sudan Zhang, Jiaren Zhang, Yi Jin. ✉e-mail: cpu_son@163.com; niujianlou@wmu.edu.cn

Notably, secretory goblet cells produce mucus and anti-microbial peptides to contribute to epithelial barrier integrity[9–11]. Numerous clinical and basic studies have demonstrated that the main pathological feature and diagnostic criteria of IBD are impaired intestinal epithelia barrier[8,12], especially goblet cell loss, which probably facilitates the access of the luminal antigens across the epithelium and thus leading to immune activation and thereby inflammation. Therefore, targeting goblet cell differentiation to promote the restitution of epithelia barrier and mucosal immunity is of great significance for restoring tissue homeostasis and alleviating inflammation, and has become a potential strategy for IBD treatment. Apart from multiple classical cytokines (including WNT, R-spondin, Notch, EGF and BMP) and their activated signaling pathways identified to regulate intestinal stem cell (ISC) self-renewal and cell lineage commitment[6,13], growing evidence have highlighted the importance of epithelial signals in regulating ISC differentiation[14–16]. However, the cytokines and signaling pathways that can precisely regulate ISC commitment toward goblet cells have not been fully elucidated.

Fibroblast growth factor 1 (FGF1) belongs to a family of eighteen different FGF proteins, which regulate a wide range of biological functions, including development, homeostasis, and disease[17]. Previous studies have shown that the physiological functions of FGF1 spans the area of wound healing, angiogenesis, skeletal muscle regeneration and cardioprotection[18], playing a key role in the repair of multiple organs or tissues after injury. However, the precise mechanism and functional role of FGF1, the most abundant FGF ligand expressed in the colon, in the pathogenesis of IBD have not been investigated. Even less is known about the effects of FGF1 on intestinal barrier restitution or its regulatory role on goblet cell differentiation during IBD.

In the present study, we showed that colonic expression of FGF1 is positively correlated with goblet cell number and inversely correlated with the severity and progression of IBD mouse models (including UC and CD models) and patients. Intestinal epithelial cell (IEC)-specific deficiency of *Fgf1* leads to impaired goblet cell differentiation and colonic epithelial barrier, exacerbating IBD phenotype; whereas pharmacological administration of recombinant FGF1 significantly improves the intestinal epithelial barrier by enhancing goblet cell differentiation, thereby alleviating IBD. In terms of molecular mechanism, FGF1 drives ISC commitment toward goblet cells by activating the FGFR2-TCF4-ATOH1 signaling axis. Taken together, we identified paracrine FGF1 as an epithelial niche-derived cytokine that drives ISC differentiation toward goblet cells, providing mechanistic insights into the pathogenesis of IBD and potential therapeutic strategies for treatment of this disease.

Results

Colonic expression level of FGF1 is negatively correlated with pathological progression of IBD in both mouse models and human patients

To investigate the role of FGFs in the occurrence and development of IBD, we analyzed the expression profile of all *Fgfs* in colon tissue of normal mice and found that *Fgf1*, *Fgf2*, *Fgf7*, *Fgf9* and *Fgf10* were abundantly expressed in colon under the steady-state conditions, while *Fgf3*, *Fgf5*, *Fgf6*, *Fgf8*, *Fgf17*, *Fgf20*, and *Fgf21* were undetectable (Supplementary Fig. 1A). Furthermore, we performed a systematic qRT-PCR analysis of the colonic expression of all *Fgfs* comparatively in response to dextran sodium sulfate (DSS) or 2,4,6-trinitrobenzene sulfonic acid (TNBS) challenge (which are known to induce ulcerative colitis (UC) and Crohn's disease (CD), respectively) with normal mice as a control. We found that, consistent with previous reports[19–21], colonic expression levels of *Fgf2*, *Fgf7* and *Fgf10* were significantly upregulated in DSS-treated UC mice (Fig. 1A and Supplementary Fig. 1B-E), but not in TNBS-induce CD mice (Fig. 1B and Supplementary Fig. 1F–I). More importantly, qRT-PCR and western blotting analysis showed that FGF1, the most predominantly expressed FGF ligand in the colon, was the unique FGF member which was commonly downregulated in both UC and CD mouse models (Fig. 1A, B and Supplementary Fig. 1E, I). Double IF staining of FGF1 and epithelial cell adhesion molecule (EpCAM, a marker of intestinal epithelial cells) or alpha-1 type 1 collagen (Col1α1, a marker of intestinal mesenchymal cells) showed that FGF1 is mainly expressed in EpCAM-positive intestinal epithelial cells (IEC), whose expression was significantly reduced in mice treated with DSS or TNBS (Fig. 1C, D and Supplementary Fig. 2A, B). Furthermore, reanalysis of single-cell RNA sequencing data (scRNA-seq, GSE264408) and double IF staining of FGF1 with different IEC markers (including Muc2, goblet cells; doublecortin-like kinase (Dclk1), tuft cells; chromogranin A (ChgA), enteroendocrine cells; fatty acid binding protein 1 (Fabp1), absorptive enterocytes) showed that colonic FGF1 is an epithelial niche-derived cytokine (Supplementary Fig. 2C–E), whose levels were generally reduced in most IEC types rather than in specific IECs in IBD mice (Supplementary Fig. 2C–E).

To further assess the clinical relevance of FGF1 with UC and CD, the expression levels of FGF1 in colon samples from UC or CD patients (stratified by differential pathological stages based on ulcerative colitis endoscopic index of severity (UCEIS) or simple endoscopic score for Crohn's disease (SES-CD)) were analyzed (Supplementary Table 1 and 2). Consistent with the results obtained from IBD mouse models, double IF staining showed the colonic levels of FGF1, mainly expressed in EpCAM-positive IECs, were significantly decreased with the progression of IBD, as revealed by a negative correlation between the colonic expressions of FGF1 and disease activity indexes (UCEIS or SES-CD) in IBD patients (Fig. 1E–G and I and Supplementary Fig. 2F–G). Besides, we observed that the colonic expressions of FGF1 were positively correlated with goblet cell numbers (lower panel in Fig. 1E, F, H and J), suggesting that FGF1 may be associated with the proliferation or differentiation of goblet cells. Taken together, all these data suggest that the reduction of IEC-derived FGF1 is probably involved in the pathogenesis of IBD.

IEC-specific deletion of *Fgf1* exacerbates DSS or TNBS-induced colitis via decreasing goblet cell number in colon

To explore the role of intestinal epithelial cells (IEC)-derived FGF1 in IBD, *Fgf1* was conditionally deleted in IECs by generating Villin-Cre+; $Fgf1^{flox/flox}$ (VilCre$Fgf1^{fl/fl}$) mice (Fig. 2A, B and Supplementary Fig. 3A), followed by DSS challenge to induce UC mouse model. We found that, under normal water, the loss of IEC-specific *Fgf1* had little effects on body weight, disease activity index, colon length and histology score. However, under the challenge of DSS, VilCre$Fgf1^{fl/fl}$ mice showed exacerbated body weight loss, increased disease activity index, colon length shortening and tissue damage in distal colon, compared to $Fgf1^{fl/fl}$ mice (Fig. 2C–F). Via analyzing the lineage markers, we found a significant reduction in goblet cell marker (*Muc2*) expression in colonic homogenates of VilCre$Fgf1^{fl/fl}$ mice treated with DSS compared to Cre-negative littermate controls ($Fgf1^{fl/fl}$ mice), whereas markers for tuft cells (*Dclk1*), enteroendocrine cells (*ChgA*) and absorptive enterocytes (*Fabp1*, *keratin 20* (*Krt20*), *apolipoprotein A1* (*Apoa1*)) did not change (Supplementary Fig. 3B). The IF staining of the above cell markers, including Muc2, Dclk1, ChgA and Fabp1, and PAS-AB staining further confirmed a specific and remarked reduction in goblet cell number in distal colon of VilCre$Fgf1^{fl/fl}$ mice compared to $Fgf1^{fl/fl}$ mice under DSS challenge (Fig. 2G–I). In addition, the bacterial 16S ribosomal RNA sequencing (to evaluate the composition of gut microbiota in colonic feces) showed that there was nearly equalized bacterial composition in VilCre$Fgf1^{fl/fl}$ and $Fgf1^{fl/fl}$ littermates (Supplementary Fig. 3C–E), suggesting that IEC-specific *Fgf1* deficiency exacerbates DSS-induced UC colitis independently of intestinal microbiota.

To further confirm the key role of IEC-specific *Fgf1* deficiency in the pathogenesis of IBD, the CD mouse colitis model was established

https://doi.org/10.1038/s41467-025-58644-2

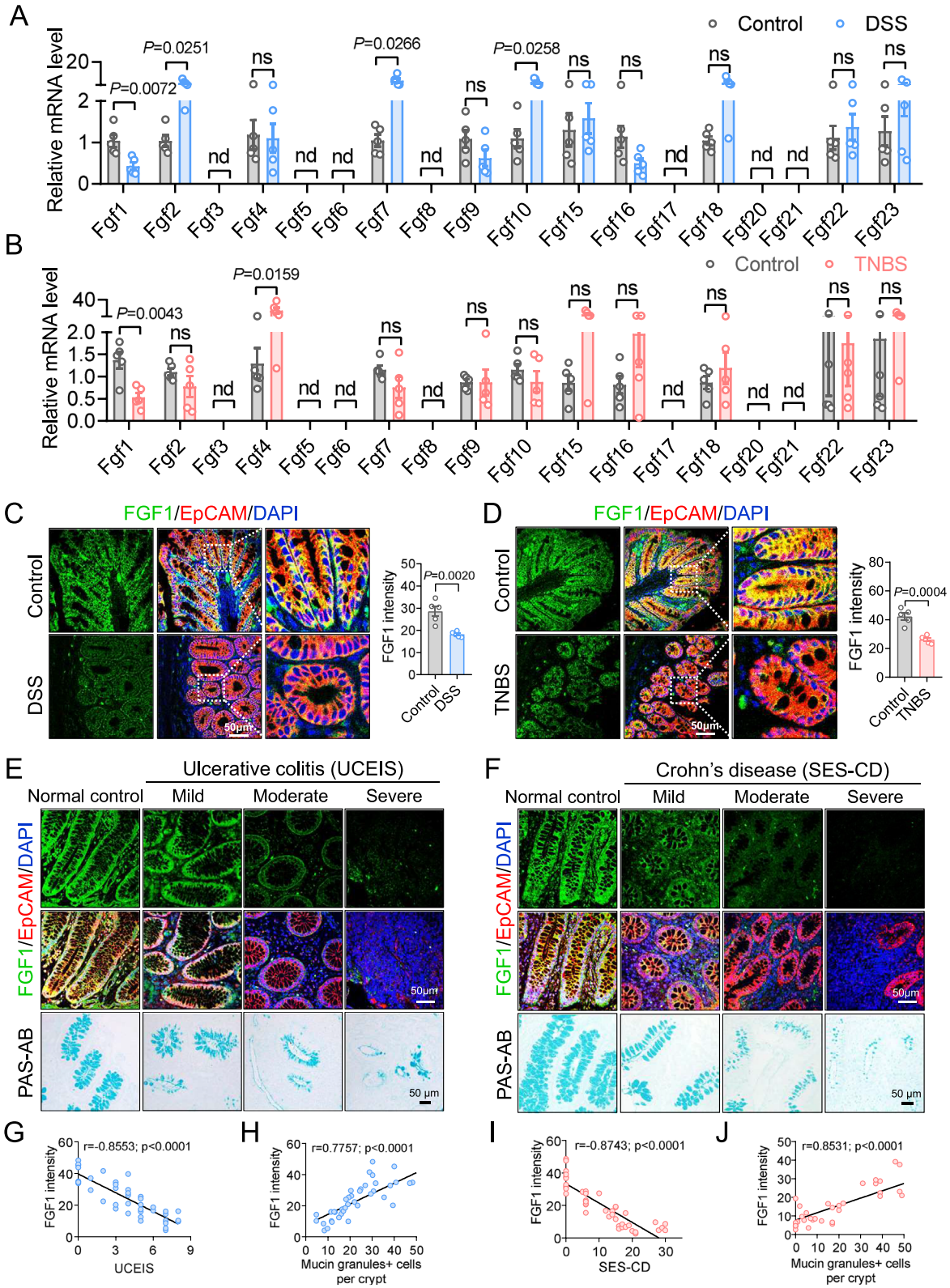

by treating mice with TNBS. As consistent with what observed in DSS-induced colitis, VilCre*Fgf1*$^{fl/fl}$ mice were more susceptible to TNBS-induced colitis compared to *Fgf1*$^{fl/fl}$ mice, as revealed by exacerbated colon shortening, colonic epithelium damage and goblet cell loss (Supplementary Fig. 4A-D). Taken together, all these data demonstrate that IEC-specific deletion of *Fgf1* aggravates the severity of DSS or TNBS-induced IBD probably via decreasing the goblet cell number.

FGF1 alleviates DSS and TNBS-induced colitis via mitigating goblet cell loss and improving colonic epithelium integrity

Since IEC-specific deficiency of *Fgf1* contributes to the pathogenesis of IBD, we further explored whether the replenishment of this protein could ameliorate the pathological changes of colon in IBD. Male C57BL/6 J mice were administrated with DSS for 7 days to induce acute colitis, followed by 4 days of recovery. These mice were

Fig. 1 | Colonic FGF1 levels negatively correlate with pathological grades of mouse model and human inflammatory bowel disease (IBD). A, **B** Relative mRNA levels of all *Fgf*s in colon tissues of C57BL/6 J mice and DSS (**A**)/TNBS (**B**)-induced colitis were determined by qRT-PCR ($n = 5$). **C**, **D** Analysis of the expression levels of FGF1 (green) and EpCAM (red) in the distal colon sections of control mice and DSS-induced UC or TNBS-induced CD mouse model by IF staining. Nuclei were labeled with 4,6-diamidino -2-phenylindole (DAPI). The FGF1 stains were quantified using ImageJ software ($n = 5$, the mean value of 2 fields in each mouse). **E**–**J** IF staining of FGF1 (upper panel) and PAS-AB staining (lower panel) of human colon sections from UC (**E**) ($n = 8$ for Healthy Control group, $n = 9$ for Mild group, $n = 15$ for Moderate group, $n = 9$ for Severe group) and CD (**F**) ($n = 10$ for Healthy Control group, $n = 8$ for Mild group, $n = 10$ for Moderate group, $n = 14$ for Severe group) patients. Correlation analysis between IF intensity of FGF1 and UCEIS (**G**)/ SEC-CD (**I**) or Mucin granules$^+$ cells per crypt in UC (**H**) and CD (**J**) patients. Human colon sections were classified by ulcerative colitis endoscopic index of severity (UCEIS) of 1-3 (mild), 4-6 (moderate) and 7-8 (severe) or simple endoscopic score for Crohn's Disease (SEC-CD) of 3-6 (mild), 7-16 (moderate) and 17-30 (severe). Data was presented as mean ± SEM. (**A**–**D**) two-tailed unpaired t-test (*Fgf22* (**A**) and *Fgf4*, *Fgf22*, *Fgf23* (**B**) using non-parametric statistical method, two-tailed Mann-Whitney Test); (**G**–**J**) Spearman's correlation. ns, not significance; nd, not detectable.

intraperitoneally injected with matured wild type FGF1 ($mFGF1^{WT}$) and previous engineered non-mitogenic FGF1 analog $FGF1^{\Delta HBS}$ (named rFGF1) daily until the end of the experiment, with PBS as a control (Fig. 3A). Results showed that $mFGF1^{WT}$ and rFGF1 have similar abilities to alleviate DSS-induced UC phenotypes, as revealed by improved body weight loss, reduced disease activity index and increased colon length (Supplementary Fig. 5A–D). With the consideration that the potent proliferation of wild type FGF1 may induce safety risks, hampering its clinical translation in the IBD treatment, we used non-mitogenic rFGF1 in the subsequent experiments. We found that administration of rFGF1 significantly restored body weight loss, colon length shortening and increased disease activity index induced by DSS (Fig. 3B–D). The H&E staining of distal colon showed that treatment of rFGF1 led to a visible reduction of inflammation and improvement of tissue integrity, reflected by a marked reduction of histology scores (Fig. 3E, F). Furthermore, PAS-AB and Muc2 IF staining showed a remarkable goblet cell recovering by rFGF1 treatment (Fig. 3E, F). Consistently, analysis of the lineage markers by qRT-PCR showed a significant replenishment of *Muc2* expression in distal colon by rFGF1 treatment, whereas expressions of *leucine rich repeat containing G protein-coupled receptor 5* (*Lgr5*) (stem cells), *Dclk1* (tuft cells), *ChgA* (enteroendocrine cells) and *Fabp1*, *Krt20* and *Apoa1* (enterocytes) were not affected (Fig. 3G). Taken together, these data indicate that rFGF1 administration compromise progressing colitis and restore the colonic epithelium integrity mainly via alleviating goblet cell loss.

We further assessed the therapeutic effect of rFGF1 on TNBS-induced colitis. BALB/c mice were treated with TNBS, followed by administration of rFGF1 with PBS as a control. We found that rFGF1 significantly elevated the survival rate of mice under TNBS challenge (Fig. 3H). In line with what we found in DSS-induced UC model, rFGF1 induced a considerable restoration of body weight loss and colon length shortening, and reduction of disease activity index (Fig. 3I–K). Histology analysis showed that rFGF1 also robustly dampened immune cell infiltration, epithelial injury, crypt hyperplasia and edema (Fig. 3L, M). Notably, PAS-AB, Muc2 IF staining and the lineage markers analysis by qRT-PCR showed that administration of rFGF1 remarkably reserve goblet cell population in the TNBS-induced colitis (Fig. 3L–N). Therefore, these data further confirm the protective role of FGF1 in IBD via mitigating goblet cell loss and improving colonic epithelium integrity.

FGF1 drives intestinal stem cell (ISC) commitment toward goblet cells

To explore the underlying mechanisms by which rFGF1 alleviated goblet cell loss in IBD mouse models, the effects of rFGF1 on IECs life cycle including proliferation and apoptosis were analyzed in vivo. We found that there were little differences in cell apoptosis (assessed by TUNEL staining) and proliferation (assessed by Ki67 staining) of colon between $Fgf1^{fl/fl}$ and VilCre$Fgf1^{fl/fl}$ mice challenged with DSS or TNBS (Supplementary Fig. 6A, B). Interestingly, administration of rFGF1 induced a dominant decrease in colonic epithelial cell proliferation in mice pretreated with DSS or TNBS (Supplementary Fig. 6C, D), probably due to that rFGF1 treatment relieved impaired epithelial barrier, which no longer requires intestinal stem cells (ISC) proliferation for repair. These data indicate that the change of IECs' proliferation is the result rather than the cause of FGF1's relief on intestinal barrier damage. Besides, rFGF1 also had no significant effect on cell apoptosis of colonic epithelial cell (Supplementary Fig. 6C, D). Furthermore, we acutely i.p. injected rFGF1 into normal C57BL/6 J mice to analyze its effects on the cell proliferation, and found that rFGF1 did not induce ISC proliferation or change the cellular composition of colonic epithelium under steady-state condition (Supplementary Fig. 7A–D). Therefore, all these data exclude the contribution of cell apoptosis and proliferation to rFGF1-induced increase in goblet cell number.

It has been previously demonstrated that enhancing goblet cell differentiation is a crucial way to elevate its number and maintain a healthy intestinal epithelium[9,10]. We found that rFGF1 administration significantly upregulated expressions of goblet cell terminal differentiation factors including E74 like ETS transcription factor 3 (Elf3) and Krüpple-like factor 4 (Klf4) in two IBD mouse models (Fig. 4A, B), indicating that rFGF1 alleviates DSS or TNBS-induced goblet cell loss probably via promoting goblet cell differentiation. To further explore the role of colonic epithelial cell-derived FGF1 in goblet cell differentiation, we isolated and cultured murine colonic organoids, a three-dimensional (3D) cell culture system in which enterocytes and secretory epithelial lineages are differentiated from primary crypts. As expected, we found that, compared to that of $Fgf1^{fl/fl}$ mice, the murine colonic organoids from VilCre$Fgf1^{fl/fl}$ mice showed a prominent decrease in the ratio of budding organoids, a hallmark of intestinal stem cell differentiation in crypts, without changing the proliferation as revealed by Ki67 IF staining (Fig. 4C). Notably, analysis of cell lineage commitment by IF staining showed that deletion of IEC-*Fgf1* specifically decreased Muc2 (goblet cell marker) level in murine colonic organoids, without changing the levels of markers for tuft cells (Dclk1), enteroendocrine cells (ChgA) or absorptive enterocytes (Fabp1) (Fig. 4D). In contrast, morphology examination of in vitro murine colonic organoids displayed that rFGF1 stimulation directly induced a significant increase in the ratio of budding organoid and had no effect on cell proliferation (Fig. 4E). Analysis of cell lineage markers by qRT-PCR and IF staining further showed that rFGF1 stimulation significantly increased the expression of Muc2 (goblet cell marker) in murine colonic organoids, but had no effects on markers for tuft cells (Dclk1), enteroendocrine cells (ChgA) and absorptive enterocytes (Fabp1, Krt20, Apoa1) (Fig. 4F–H). More importantly, we also found that rFGF1 treatment induced goblet cell differentiation in human colonic organoids with vehicle as a control, which was in line with our findings in murine colonic organoids (Fig. 4I–L). Taken together, these data provide direct evidence that rFGF1 drives ISC differentiation toward goblet cells.

ATOH1 mediates the regulation of FGF1 in driving ISC differentiation toward goblet cells

To investigate how rFGF1 promotes ISC differentiation toward goblet cells, we analyzed the PBS or rFGF1-treated UC mice by RNA sequencing and found that 602 genes were downregulated, whereas 174 genes were upregulated (based on fold change > 2 and p value < 0.05), as shown in the volcano plot (Supplementary Fig. 8A). The KEGG enrichment analysis of the differential genes further revealed that rFGF1 significantly upregulated multiple genes belonging to "Protein

https://doi.org/10.1038/s41467-025-58644-2

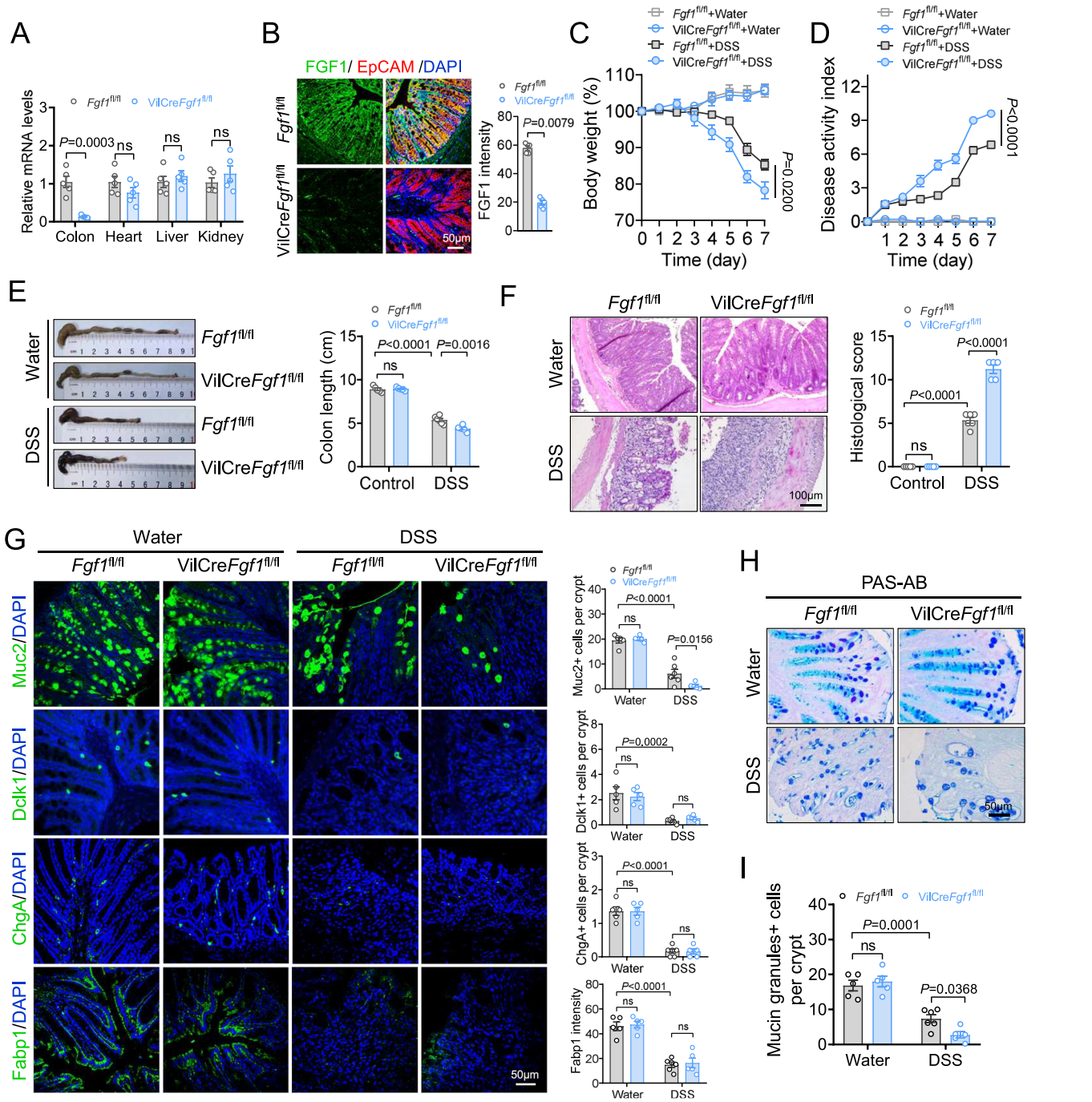

Fig. 2 | Deficiency of *Fgf1* in intestinal epithelial cells sensitizes mice to DSS-induced colitis. A, **B** Deficiency of *Fgf1* in IECs was verified by qRT-PCR (**A**) and IF staining (**B**) ($n = 5$). **C**–**E** Weight loss (**C**), disease activity index (**D**) and colon length (**E**) of $Fgf1^{fl/fl}$ and VilCre$Fgf1^{fl/fl}$ mice that received regular drinking water with or without 2.5% DSS for 7 days. The distal colon tissues were collected and analyzed at the end of this experiment ($n = 6$ for $Fgf1^{fl/fl}$ + DSS group, $n = 5$ for other groups). **F** H&E staining of distal colon sections of $Fgf1^{fl/fl}$ and VilCre$Fgf1^{fl/fl}$ mice with or without DSS challenge and its histology score ($n = 6$ for $Fgf1^{fl/fl}$ + DSS group, $n = 5$ for other groups). **G** Goblet (Muc2$^+$, in green), tuft (Dclk1$^+$, in green), enteroendocrine (ChgA$^+$, in green) and absorptive enterocyte (Fabp1$^+$, in green) cells were quantified by IF staining of the distal colon sections of $Fgf1^{fl/fl}$ and VilCre$Fgf1^{fl/fl}$ mice with or without DSS challenge ($n = 6$ for $Fgf1^{fl/fl}$ + DSS group, $n = 5$ for other groups). **H**–**I** PAS-AB staining of the distal colon sections of $Fgf1^{fl/fl}$ and VilCre$Fgf1^{fl/fl}$ mice with or without DSS challenge (**H**). Mucin granules$^+$ cells per crypt were counted (**I**) ($n = 6$ for $Fgf1^{fl/fl}$ + DSS group, $n = 5$ for other groups). Data was presented as mean ± SEM. (**A**, right panel of **B**) two-tailed unpaired *t*-test (kidney (**A**) using non-parametric statistical method, two-tailed Mann-Whitney Test); (**C**, **D**) *P* values on day 7 were calculated using ordinary two-way ANOVA, followed by Sidak; (right panel of **E**–**G**, **I**) ordinary two-way ANOVA, followed by Sidak. ns, not significance.

digestion and absorption", "ECM-receptor interaction" and "Focal adhesion" pathways, suggesting that rFGF1 treatment reconstructed intestinal epithelial barrier and restored intestinal absorption function (Supplementary Fig. 8B). It is worth noting that rFGF1 treatment significantly upregulated atonal BHLH transcription factor 1 (ATOH1), the most important transcription factor that promotes Lgr5$^+$ intestinal stem cells (ISC) differentiation toward secretory lineage[16,22,23], which was further validated in DSS or TNBS-induced colitis mouse models by

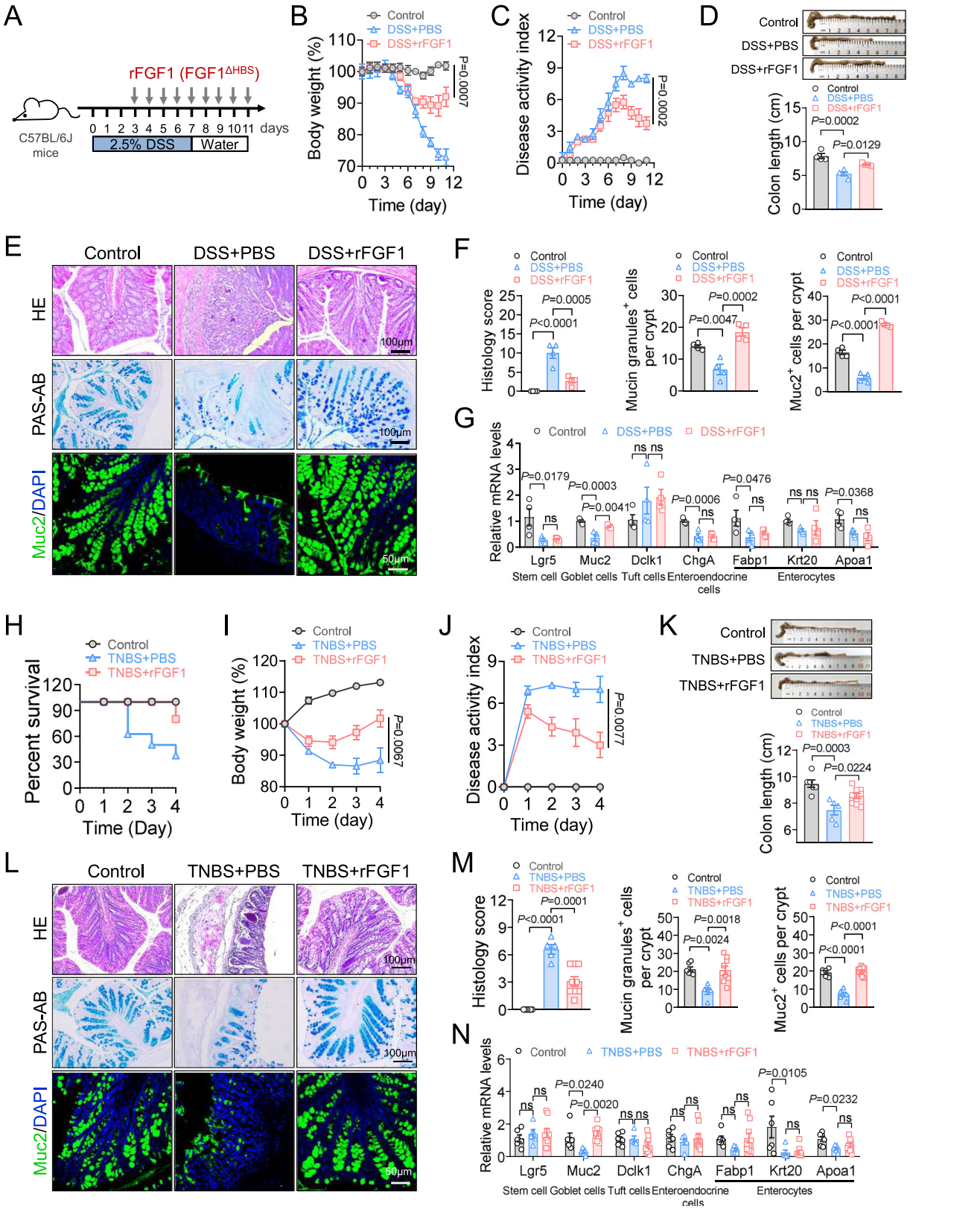

qRT-PCR (Fig. 5A). Notably, several downstream target genes of ATOH1, especially goblet cell differentiation-related genes (*Spdef* and *Sox9*)[24–26] were significantly upregulated (Fig. 5A), while transcription factors important for specification of other cell lineages, such as *Neurog 3* and *Gfi1* (EECs), *Pou2f3* and *Sox4* (tuft cells), hepatocyte nuclear factor *4α* (HNF4α) and *HNF4γ* (enterocytes), did not change (Supplementary Fig. 8C). Besides, we found that, IEC-specific *Fgf1* deficiency led to a remarked reduction of colonic ATOH1 expression under the challenge of DSS or TNBS (Fig. 5B, C). In contrast, rFGF1 treatment significantly increased colonic ATOH1 expression in UC and CD mouse models (Fig. 5D, E). Thus, these data confirmed that IEC-derived FGF1 is an upstream activator of ATOH1 during IBD.

Fig. 3 | Administration of rFGF1 increased goblet cell number and improved the epithelium integrity to resist DSS or TNBS-induced colitis. A The experimental design. C57BL/6 J mice received regular drinking water with or without 2.5% DSS for 7 days, and daily i.p. injected with PBS or rFGF1 starting from the third day until the end of this experiment. The distal colon tissues were collected and analyzed at the end of this experiment ($n = 4$). **B**–**D** Weight loss (**B**) disease activity index (**C**) colon length (**D**) ($n = 4$). **E**, **F** H&E (upper panel), PAS-AB staining (middle panel) and Muc2 IF staining (lower panel) of distal colon sections (**E**). Histology scores (left panel; $n = 4$), counting of mucin granules-positive cells per crypt (middle panel; $n = 4$) and Muc2-positive cells per crypt (right panel; $n = 4$) of distal colon sections (**F**). **G** Colonic stem cells (*Lgr5*), goblet cells (*Muc2*), Tuft cells (*Dclk1*), enteroendocrine cells (*ChgA*) and absorptive enterocytes (*Fabp1*, *Krt20*, *Apoa1*) markers were determined by qRT-PCR ($n = 4$). **H**–**K** BALB/c mice were rectally administered with TNBS, followed by PBS or rFGF1 injection. The survival rates (**H**) weight loss (**I**) disease activity index (**J**) and colon length (**K**) of mice were measured. The distal colon tissues were collected and analyzed at the end of this experiment ($n = 6$ for Control group, $n = 5$ for TNBS + PBS group, $n = 9$ for TNBS + rFGF1 group). **L**–**M** H&E (upper panel), PAS-AB staining (middle panel) and Muc2 IF staining (lower panel) of distal colon sections (**L**). Histology scores (left panel), counting of mucin granules-positive cells per crypt (middle panel) and counting of muc2-positive cells per crypt (right panel) of distal colon sections (**M**) ($n = 6$ for Control group, $n = 5$ for TNBS + PBS group, $n = 9$ for TNBS + rFGF1 group). **N** Colonic stem cells (*Lgr5*), goblet cells (*Muc2*), tuft cells (*Dclk1*), enteroendocrine cells (*ChgA*) and absorptive enterocytes (*Fabp1*, *Krt20*, *Apoa1*) markers were determined by qRT-PCR ($n = 6$ for Control group, $n = 5$ for TNBS + PBS group, n = 9 for TNBS + rFGF1 group). Data was presented as mean ± SEM. (**B**–**C**) P values on day 12 were calculated using ordinary one-way ANOVA, followed by Dunnett; (**I**–**J**) *P* values on day 4 were calculated using ordinary one-way ANOVA, followed by Dunnett; (**D**–**G**, **K**–**N**) ordinary one-way ANOVA, followed by Dunnet (*Muc2*, *Dclk1*, *ChgA* and *Krt20* (**N**) using non-parametric statistical method, Kruskal Willis Test with a post hoc Dunn's test). ns, not significance; nd, not detectable.

To further explore the role of ATOH1 in FGF1-mediated ISC differentiation toward goblet cell, murine colonic organoids were transfected with shRNA to knock-down *Atoh1* expression, followed by rFGF1 stimulation. We found that rFGF1 failed to induce budding of organoids after transfected with sh*Atoh1* (upper panel, Fig. 5F). Knock-down of *Atoh1* largely compromised basal levels of Muc2 expression in colonic organoids (lower panel in Fig. 5F). More importantly, rFGF1 increase Muc2 (goblet cell marker) level in shNC, but not sh*Atoh1* transfected organoids (lower panel in Fig. 5F). In addition, rFGF1 stimulation did not change markers for tuft cells (Dclk1), enteroendocrine cells (ChgA) and absorptive enterocytes (Fabp1) in shNC and sh*Atoh1* (Supplementary Fig. 8D). Furthermore, PAS-AB and Muc2 IF staining of distal colon tissues from *VilCreAtoh1*$^{+/-}$ heterozygous knockout mice showed that, under the challenge of DSS, 50% knocking out of *Atoh1* in IECs reduced basal Muc2 expression levels. Notably, the increased goblet cell number induced by rFGF1 was significantly attenuated in *VilCreAtoh1*$^{+/-}$ heterozygous knockout mice, as revealed by Muc2 IF and PAS-AB staining (Supplementary Fig. 8E, F). Since IEC-specific deletion of *Atoh1* is lethal, we generated tamoxifen-inducible knockout Villin-Cre^{ERT2}*Atoh1*$^{fl/fl}$ mice and confirmed that injection of tamoxifen in Villin-Cre^{ERT2}*Atoh1*$^{fl/fl}$ mice led to remarkable reduction in *Atoh1* expression (as determined by qRT-PCR and IF staining) (Fig. 5G, H). Although administration of rFGF1 significantly restored DSS-induced body weight loss, colon length shortening and increased disease activity index in control Villin-Cre^{ERT2}*Atoh1*$^{fl/fl}$ mice, all these beneficial effects were lost in tamoxifen treated Villin-Cre^{ERT2}*Atoh1*$^{fl/fl}$ mice (Fig. 5I–M). Notably, FGF1-induced goblet cell differentiation is also compromised in Villin-Cre^{ERT2}*Atoh1*$^{fl/fl}$ mice (Fig. 5M). In summary, combined with the results of FGF1 stimulation in organoids in vitro (Fig. 4), these data strongly support that ATOH1 mediates the regulation of FGF1 in driving ISC differentiation toward goblet cells.

Given that ATOH1 is regulated by Notch signaling pathway[6,27,28], we further explored whether the Notch mediated ATOH1 activation by rFGF1. However, we found that Notch ligands (Dll1 and Dll4) and the Notch effector Hes1 were not different in DSS-induced UC mouse models after FGF1 treatment (Supplementary Fig. 9A). Consistently, rFGF1 did not change the levels of activated form of Notch 1 (cleaved Notch 1 intracellular domain, NICD) in DSS-induced colitis mice (Supplementary Fig. 9B). Furthermore, the mRNA and protein levels of β-catenin and axin2 remained unchanged after rFGF1 treatment in UC moues models (Supplementary Fig. 9C-D).

TCF4 mediates the transcriptional upregulation of *Atoh1* by FGF1

To identify the nuclear factors that mediate the transcriptional regulation of *Atoh1* by rFGF1, we intersected differentially expressed genes in the colon tissues of FGF1-treated UC mice with the predicted transcription factors that could regulated *Atoh1*, and found seven potential nuclear transcription factors, including *Kdm1a*, *Hoxa13*, *Tec*, *Nfya*, *Nr4a1*, *Tcf4* and *Ncaph2* (Fig. 6A). The results of qRT-PCR showed that only *transcription factor 4* (*Tcf4*) was significantly upregulated by rFGF1 treatment (Fig. 6B). In contrast, we found a significant reduction of TCF4 expression in colonic homogenates of VilCre*Fgf1*$^{fl/fl}$ mice challenged with DSS or TNBS compared to *Fgf1*$^{fl/fl}$ mice (Fig. 6C, D). The upregulation of TCF4 induced by rFGF1 was further confirmed in two IBD mouse models (UC and CD) (Fig. 6E, F). In addition, consistent with IF staining results showing that TCF4 localized at the base of the crypt, scRNA analysis of *Tcf4* expression profile indicated that *Tcf4* was highly expressed in intestinal stem cells (ISCs) (Supplementary Fig. 10A). To verify whether TCF4 was involved in the transcriptional regulation of *Atoh1*, potential binding sites of TCF4 in the promoter region of *Atoh1* were predicted using JASPAR database (Fig. 6G, left panel). We then generated plasmids expressing wild-type or double-site mutant *Atoh1* promoter based on predicted binding sites of TCF4 (Fig. 6G, right panel). After transfecting HT-29 cells with a *Tcf4* overexpression plasmid and a plasmid encoding human wild-type (WT) or mutant *Atoh1* promoter (M1, M2, M3), luciferase reporter assay showed that TCF4 significantly induced the activity of wild-type *Atoh1* promoter but not M3 mutant (Fig. 6H). Furthermore, we found that the luciferase activity was significantly abolished in HT-29 cells transfected with M3-1 or M3-2 mutant compared to WT control, identifying both motifs as the binding site of the ATOH1-TCF4 complex (Fig. 6I). This result was further confirmed via chromatin immunoprecipitation (ChIP) experiments which showed that TCF4 bound to the *Atoh1* promoter (Fig. 6J). More importantly, the upregulation of ATOH1, Muc2 expression and the ratio of budding organoids induced by rFGF1 were abolished in sh*Tcf4*-transfeceted organoids (Fig. 6K, L). Taken together, all these data strongly demonstrate that TCF4 mediates the transcriptional upregulation of *Atoh1* by FGF1.

FGF1 acts on FGFR2 in Lgr5^{+}ISCs to activate TCF4-ATOH1 signaling axis-mediated goblet cell differentiation

It has been reported that FGF1 ubiquitously binds to all FGF receptors (FGFRs) to initiate intracellular signaling[17,29]. To explore the exact FGFR involved in FGF1's regulation on ISCs differentiation toward goblet cells, we reanalyzed a single-cell RNA sequencing dataset (scRNA-seq, GSM4983265) and found that *Fgfr2* was higher expressed in ISCs than other *Fgfrs* (Fig. 7A). The IF staining showed that FGFR2 was mainly expressed at the bottom of crypts and overlapped with Lgr5^{+} ISCs (Fig. 7B), suggesting that FGFR2 expressed in Lgr5^{+} ISCs may mediate the role of FGF1 in promoting goblet cell differentiation. To further explore this notion, colonic organoids derived from Lgr5-EGFP-Cre^{ERT2} *Fgfr2*$^{fl/fl}$ mice were stimulated with rFGF1 for 7 days. We found that rFGF1 upregulated the ratio of budding organoids derived from control Lgr5-EGFP-Cre^{ERT2}*Fgfr2*$^{fl/fl}$ mice without tamoxifen treatment, but not from *Fgfr2*-deficient Lgr5-EGFP-Cre^{ERT2}*Fgfr2*$^{fl/fl}$ mice treated by

https://doi.org/10.1038/s41467-025-58644-2

tamoxifen (Fig. 7C, D). Of note, rFGF1 failed to induce TCF4-ATOH1 signaling axis and Muc2 expression in colonic organoids from *Fgfr2*-deficient Lgr5-EGFP-Cre^{ERT2}*Fgfr2*$^{fl/fl}$ mice (Fig. 7D). Collectively, these results suggest that FGFR2 in Lgr5^{+} ISCs mediates the role of FGF1 in promoting TCF4-ATOH1 axis-mediated goblet cell differentiation. In addition, we observed that the size of organoid extracted from TAM-

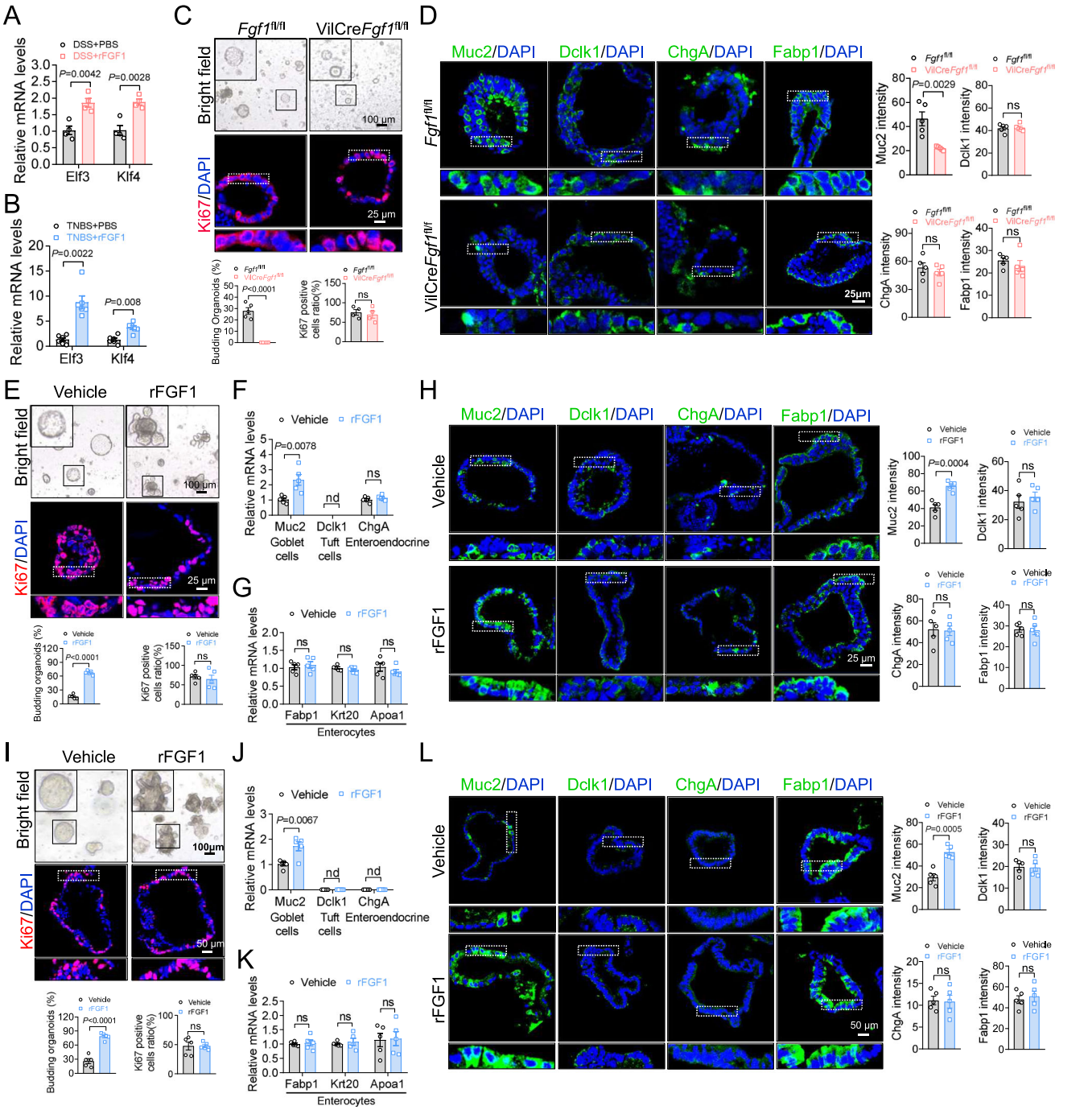

Fig. 4 | FGF1 drives intestinal stem cell differentiation toward goblet cells. **A**, **B** qRT-PCR analysis of *Elf3* and *Klf4* mRNA levels in distal colon sections of DSS (**A**, $n = 4$) or TNBS (**B**, $n = 6$) induced IBD mouse models treatment with PBS or rFGF1. **C** Representative images (upper panel, $n = 5$) and IF staining of Ki67 (lower panel, $n = 4$) in murine colonic organoids derived from *Fgf1*$^{fl/fl}$ and VilCre*Fgf1*$^{fl/fl}$ mice were cultured for 7 days and analyzed. **D** Goblet cells (Muc2^{+}, in green), tuft cells (Dclk1^{+}, in green), enteroendocrine cells (ChgA^{+}, in green) and absorptive enterocyte (Fabp1^{+}, in green) cells in colonic organoids derived from *Fgf1*$^{fl/fl}$ and VilCre*Fgf1*$^{fl/fl}$ mice were quantified by IF staining ($n = 5$). **E**–**H** Colonic organoids from normal C57BL/6 J mice were cultured and stimulated with vehicle or rFGF1 for 7 days ($n = 5$). **E** Representative images (upper panel) and Ki67 IF staining (lower panel) of murine colonic organoids. **F**, **G** The mRNA levels of *Muc2*, *ChgA*, *Dclk1* (**F**) and *Fabp1*, *Krt20* and *Apoa1* (**G**) in colonic organoids were analyzed by qRT-PCR.**H** Goblet cells (Muc2^{+}, in green), tuft cells (Dclk1^{+}, in green), enteroendocrine cells (ChgA^{+}, in green) and absorptive enterocyte (Fabp1^{+}, in green) cells were quantified by IF staining and its semi-quantitation of IF intensity. **I**–**L** Human colonic organoids were cultured and stimulated with vehicle or rFGF1 for 7 days ($n = 5$). **I** Representative images (upper panel) and Ki67 IF staining (lower panel) of human colonic organoids. **J**, **K** The mRNA levels of *Muc2*, *ChgA*, *Dclk1* (**J**) and *Fabp1*, *Krt20* and *Apoa1* (**K**) in human colonic organoids were analyzed by qRT-PCR.**L** Goblet cells (Muc2^{+}, in green), tuft cells (Dclk1^{+}, in green), enteroendocrine cells (ChgA^{+}, in green) and absorptive enterocyte (Fabp1^{+}, in green) cells were quantified by IF staining and its semi-quantitation of IF intensity. Data was presented as mean ± SEM. (**A**–**B**, **F**–**G**, **J**–**K**, lower panel of **C**, **E**, **I**, right panel of **D**, **H**, **L**) two-tailed unpaired *t*-test (*Elf3* (**B**) and *Apoa1* (**G**) using non-parametric statistical method, two-tailed Mann-Whitney Test). ns, not significance; nd, not detectable.

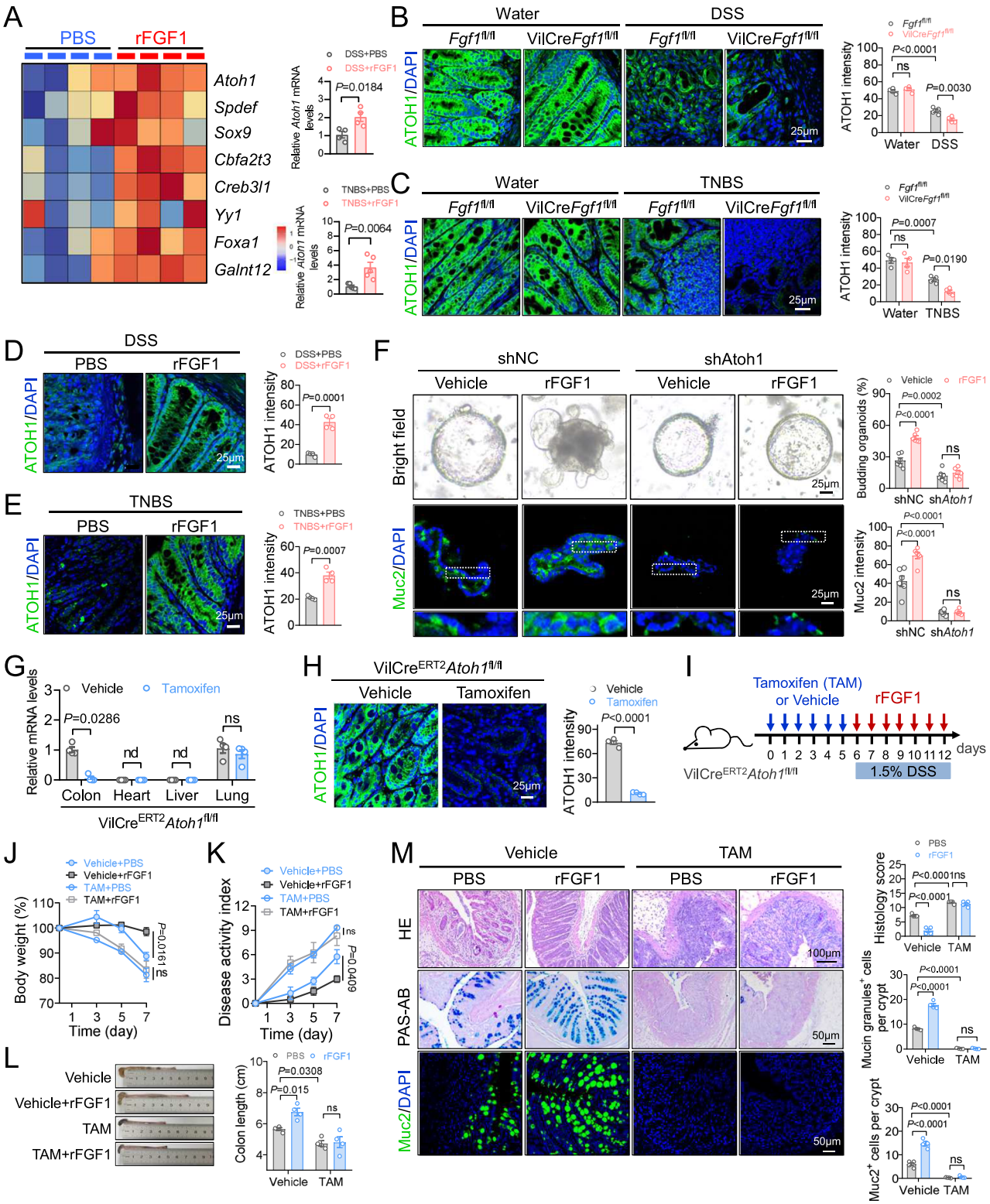

treated Lgr5-EGFP-Cre^{ERT2}*Fgfr2*$^{fl/fl}$ mice was slightly smaller than that of untreated Lgr5-EGFP-Cre^{ERT2}*Fgfr2*$^{fl/fl}$ mice, suggesting that autocrine FGF ligands may be present in crypts to promote organoid growth via activating FGFR2.

Next, we further investigated how FGFR2 regulated TCF4-ATOH1 signaling axis-mediated goblet cell differentiation. Activation of mitogen-activated protein kinase (MAPK), a well-established FGFRs' downstream[30,31], has been reported to enhance goblet cells differentiation[32]. The western blot analysis showed that rFGF1 treatment significantly increased pERK1/2 levels in colon tissues (Supplementary Fig. 11A). In colonic organoids, we found that rFGF1 lost its capacity to induce organoids budding, activate TCF4-ATOH1 signaling axis and upregulate Muc2 expression in the presence of ERK1/2 inhibitor U0126 (Supplementary Fig. 11B, C). These findings demonstrate that the FGF1 acts on Lgr5^{+} ISCs to activate FGFR2-ERK1/2-TCF4-ATOH1 signaling axis and initiate goblet cell differentiation.

To further demonstrate that FGF1 directly acts on intestinal stem cells to exert the therapeutic effect in IBD in vivo, we firstly verified that

Fig. 5 | ATOH1 is required for enhanced goblet cell differentiation induced by rFGF1. A Heatmap of differentially expressed *Atoh1* and its downstream target genes in PBS and rFGF1-treated UC mice ($n = 4$). The mRNA level of *Atoh1* in PBS or rFGF1-treated UC mice (upper panel, $n = 4$) and CD mice (lower panel, $n = 5$) was detected by qRT-PCR. **B**, **C** IF staining of ATOH1 in distal colon sections of *Fgf1*$^{fl/fl}$ and VilCre*Fgf1*$^{fl/fl}$ mice challenged with DSS (**B**) or TNBS (**C**), and its semi-quantitation of IF intensity ($n = 4$, the mean value of 2 fields in each mouse). **D**, **E** IF staining of ATOH1 in distal colon sections of DSS (**D**) or TNBS (**E**)-induced two IBD mouse models, followed by PBS or rFGF1 treatment and its semi-quantitation of IF intensity ($n = 4$, the mean value of 2 fields in each mouse). **F** Representative images (upper panel) and IF staining of Muc2 (lower panel) in sh*Atoh1* or shNC-transfected colonic organoids stimulated with vehicle or rFGF1 ($n = 6$). **G**, **H** Deletion of *Atoh1* in VilCre^{ERT2}*Atoh1*$^{fl/fl}$ mice was confirmed by qRT-PCR (**G**) and IF staining of colon tissues (**H**) ($n = 4$). **I**–**M** VilCre^{ERT2}*Atoh1*$^{fl/fl}$ mice were injected with tamoxifen for five consecutive days and then given drinking water containing 1.5% DSS to induce acute colitis, followed by vehicle or rFGF1 administration for 7 days. At end of the experiment, the distal colon tissues were harvested and examined. The schematic diagram shows the strategy of tamoxifen injection, DSS challenge and rFGF1 administration ($n = 4$). **J**–**L** Weight loss (**J**), disease activity index (**K**), colonic length (**L**) were monitored (n = 4). **M** H&E (upper panel), PAS-AB staining (middle panel) and Muc2 IF staining (lower panel) of distal colon sections ($n = 4$). Data was presented as mean ± SEM. (**A**, **D**–**E**, **H**) two-tailed unpaired *t*-test; (**B**, **C**, **F**, **J**–**M**) ordinary two-way ANOVA, followed by Sidak; (**G**) Non-parametric statistical method, two-tailed Mann-Whitney test. ns, not significance; nd, not detectable.

TAM injection achieves inducible knockout of *Fgfr2* in the intestinal epithelium (Fig. 7C and Supplementary Fig. 12A). We found no macroscopic structural or cellular abnormality in Lgr5-EGFP-Cre^{ERT2}*Fgfr2*$^{fl/fl}$ mice after TAM injection under homeostatic conditions (Supplementary Fig. 12B, C). As expected, under the challenge of DSS, we observed that rFGF1 treatment failed to improve body weight loss, colon length shortening and disease activity index in tamoxifen-treated Lgr5-EGFP-Cre^{ERT2}*Fgfr2*$^{fl/fl}$ mice (Fig. 7E–G). H&E, PAS-AB and Muc2 IF staining showed that rFGF1 treatment failed to improve DSS-induced epithelial damage and goblet cell loss in tamoxifen-treated Lgr5-EGFP-Cre^{ERT2}*Fgfr2*$^{fl/fl}$ mice (Fig. 7H, I). Consistently, IF staining showed that rFGF1 treatment did not upregulate the TCF4 and ATOH1 expressions in the Lgr5-EGFP-Cre^{ERT2}*Fgfr2*$^{fl/fl}$ mice (Fig. 7I). Taken together, all these data demonstrate that the deficiency of *Fgfr2* in Lgr5^{+} ISCs abolished the effect of rFGF1 in promoting goblet cell differentiation and protecting DSS-induced colitis.

In addition, via analyzing the results of single-cell sequencing of colon tissues from UC mouse model and IBD patients (Supplementary Fig. 13A–C), we found that levels of *Tcf4* and *Atoh1* in ISCs were significantly downregulated probably due to decreased IEC-derived FGF1 after IBD onset. This result further supports our proposal that IEC-derived FGF1 drives Tcf4-Atoh1 signaling axis-mediated stem cell differentiation in the ISCs.

Discussion

Intestinal stem cell (ISC) self-renewal and cell lineage commitment after leaving crypts are essential for maintaining intestinal barrier and mucosal immunity during hemostasis and following tissue injury[33–35]. Numerous studies have shown the intestinal stem cell niche consists of an epithelial component, provided by Paneth cells in the small intestine and a mesenchymal component that provides WNT pathway activation, EGF signaling and BMP inhibition[6,36]. However, the nature and cell source of signals that drive lineage-directed differentiation of ISCs after colitis remain unclear. Here, we identified paracrine FGF1 as an epithelial niche-derived cytokine that drives ISC differentiation toward goblet cells via activating FGFR2-TCF4-ATOH1 signaling axis.

In view of the fact that the significant efficacy of FGFs in the repair of epithelial cells in skin tissue, the role of FGFs in repairing and reconstruction of intestines after injury has attracted attention many years ago. FGF2[19], FGF7[20] and FGF10[21] were found to be significantly upregulated in IBD mouse models and patients. However, studies on molecular mechanism showed that these FGFs protected intestinal epithelial barrier in murine colitis models by promoting proliferation or inhibiting apoptosis of intestinal epithelial cells (IECs). In contrast, our study demonstrates that rFGF1 promotes intestinal barrier remodeling by driving intestinal stem cell (ISC) differentiation toward goblet cells, rather than increasing epithelial cell proliferation (Fig. 4 and Supplementary Figs. 6 and 7), making FGF1-based biologics a promising therapeutic target for the treatment of IBD. In addition, the non-mitogenic rFGF1 has similar ability to alleviate intestinal barrier damage and IBD phenotypes as mFGF1^{WT} (Supplementary Fig. 5), further confirming that the therapeutic effect of FGF1 on IBD is independent of its proliferation activity.

Paracrine FGF1 plays critical roles in repair and regeneration of multiple major organs or tissues after injury[18,30]. However, the role of FGF1 in intestinal epithelial barrier dysfunction during IBD has not been investigated. Even less is known about the functional role of FGF1 in regulating intestinal stem cell (ISC) differentiation. In this study, we observed that IEC-specific *Fgf1* deletion leads to impaired goblet cell differentiation, thereby exacerbating intestinal barrier damage and the severity of DSS or TNBS-induced colitis (Fig. 2 and Supplementary Fig. 4). In contrast, administration of rFGF1 enhanced goblet cell differentiation, thereby improving colonic epithelial integrity (Fig. 3). Lineage commitment analysis using in vitro colonic organoids provided direct evidence that FGF1 drives ISC differentiation specifically toward goblet cells (Fig. 4). The positive correlation between FGF1 expression and goblet cell number in colonic tissue from IBD patients further supports this notion (Fig. 1).

ATOH1 is the major transcription factor that drives the differentiation of intestinal Lgr5^{+} stem cells toward the secretory lineage and is highly expressed in progenitor cells derived from Lgr5^{+} ISCs[6,16,22,23]. Previous studies have shown that Atoh1^{+} cells with stem cell properties are involved in epithelial regeneration after injury[37], which is critical for protecting the integrity of intestinal epithelial barrier. Our data showed that IEC-specific *Fgf1* deficiency significantly reduced ATOH1 expression in DSS or TNBS-induced IBD mouse models. Conversely, FGF1 treatment significantly upregulated the expression of ATOH1 and two goblet cell terminal differentiation factors, Elf3 and Klf4 (Fig. 4). ShRNA *Atoh1*-transfected colonic organoids and inducible IEC-*Atoh1* deficient mice (Villin-Cre^{ERT2}*Atoh1*$^{fl/fl}$) experiments demonstrated that upregulation of ATOH1 is required for the effects of rFGF1-induced ISC differentiation toward goblet cells (Fig. 5). Furthermore, we identified the connection between FGF1 and ATOH1, namely the FGFR2-ERK1/2-TCF4 signaling axis (Figs. 6 and 7 and Supplementary Fig. 11).

This study identified TCF4 as a nuclear transcription factor that regulates ATOH1 expression. However, as widely expressed in various IEC cells, TCF4 can only regulate ATOH1 expression in intestinal stem cells (ISCs), suggesting that TCF4-mediated transcriptional regulation of ATOH1 may require the assistance of some unknown molecular elements specifically expressed in ISCs. In addition, we found that ERK1/2, as a downstream signal of FGFRs, regulated the expression of TCF4, whose molecular mechanism still needs to be explored in the future.

Our findings in animal models and human-derived organoids suggest that FGF1-based therapies have the potential to be applied in the treatment of IBD patients. However, there are still several issues that need to be addressed. Firstly, the results of scRNA-seq re-analysis showed that the reduced FGF1 expression in intestinal epithelium of IBD models is probably due to the loss of IEC cells, however other possible mechanisms may also be involved and need to be elucidated in the future. Secondly, it is still unavoidable that the administration of non-mitogenic FGF1$^{\Delta HBS}$ activated widely distributed FGFRs signaling in vivo, which may induce potential

https://doi.org/10.1038/s41467-025-58644-2

toxic side effects, since mutations in heparin binding sites do not alter FGFRs selectivity. Therefore, more sophisticated protein design based on structure or artificial intelligence is needed to obtain FGF1 allosteres that preferentially activate FGFR2, or to develop delivery strategies that specifically target intestine or even intestinal stem cells to minimize off-target effects and side

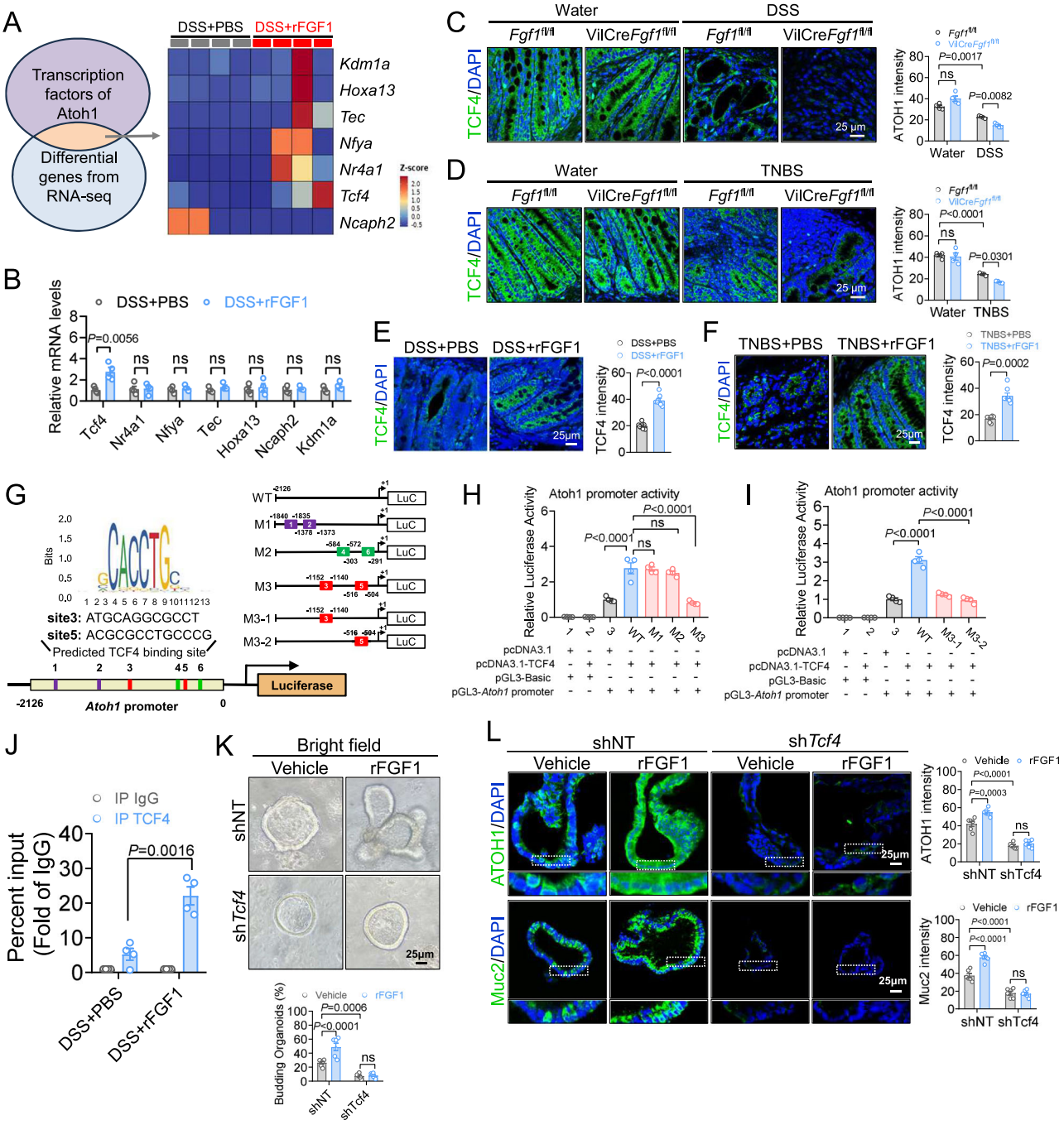

Fig. 6 | TCF4 mediates the transcriptional regulation of *Atoh1* by FGF1. **A** Workflow to find the rFGF1-regulated potential transcription factors of *Atoh1*, and heatmap of expression level of potential transcription factors ($n = 4$). **B** The expression levels of potential transcription factors of *Atoh1* (*Tcf4*, *Nr4a1*, *Nfya*, *Tec*, *Hoxa13*, *Ncaph2*, *Kdm1a*) in distal colon sections of PBS or rFGF1-treated UC mice were analyzed by qRT-PCR ($n = 4$). **C**, **D** IF staining of TCF4 in distal colon sections of *Fgf1*$^{fl/fl}$ and VilCre*Fgf1*$^{fl/fl}$ mice challenged with DSS (**C**) or TNBS (**D**) and its semi-quantitation of IF intensity ($n = 4$, the mean value of 2 fields in each mouse). **E**, **F** The expression levels of TCF4 in distal colon sections of DSS-treated UC mice (**E**) and TNBS-treated CD mice (**F**) after PBS or rFGF1 administration and IF staining ($n = 8$). **G** Predicted TCF4 binding sites on the promoter of *Atoh1* by the JASPAR database (left panel). Six binding sites with the most significant prediction scores were selected for pairwise deletion mutation analysis (right panel; M1, in purple; M2, in green; M3, in red). **H**, **I** Luciferase activity in HT-29 cells transfected with a human *Atoh1* promoter reporter plasmid or the predicted TCF4 binding site mutant reporter along with a *Tcf4* overexpression plasmid ($n = 4$). **J** ChIP experiments. The data were normalized to the corresponding IgG ($n = 4$). **K** Images of murine colonic organoids transfected small hairpin RNA targeting *Tcf4* (sh*Tcf4*) or negative control hairpin (shNT) followed by treated with rFGF1 or vehicle ($n = 6$). **L** IF staining of ATOH1 (upper panel) and Muc2 (lower panel) in colonic organoids in different groups and its semi-quantitation of fluorescent intensity ($n = 6$). Data was presented as mean ± SEM. (**B**, right panel of **E**–**F**, **J**) two-tailed unpaired *t*-test (*Tec* and *Ncaph2* in penal **B** using non-parametric statistical method, two-tailed Mann-Whitney Test); (**H**–**I**) ordinary one-way ANOVA, followed by Dunnett; (right panel of **C**–**D** and **L**, lower panel of **K**) ordinary two-way ANOVA, followed by Sidak. ns, no significance.

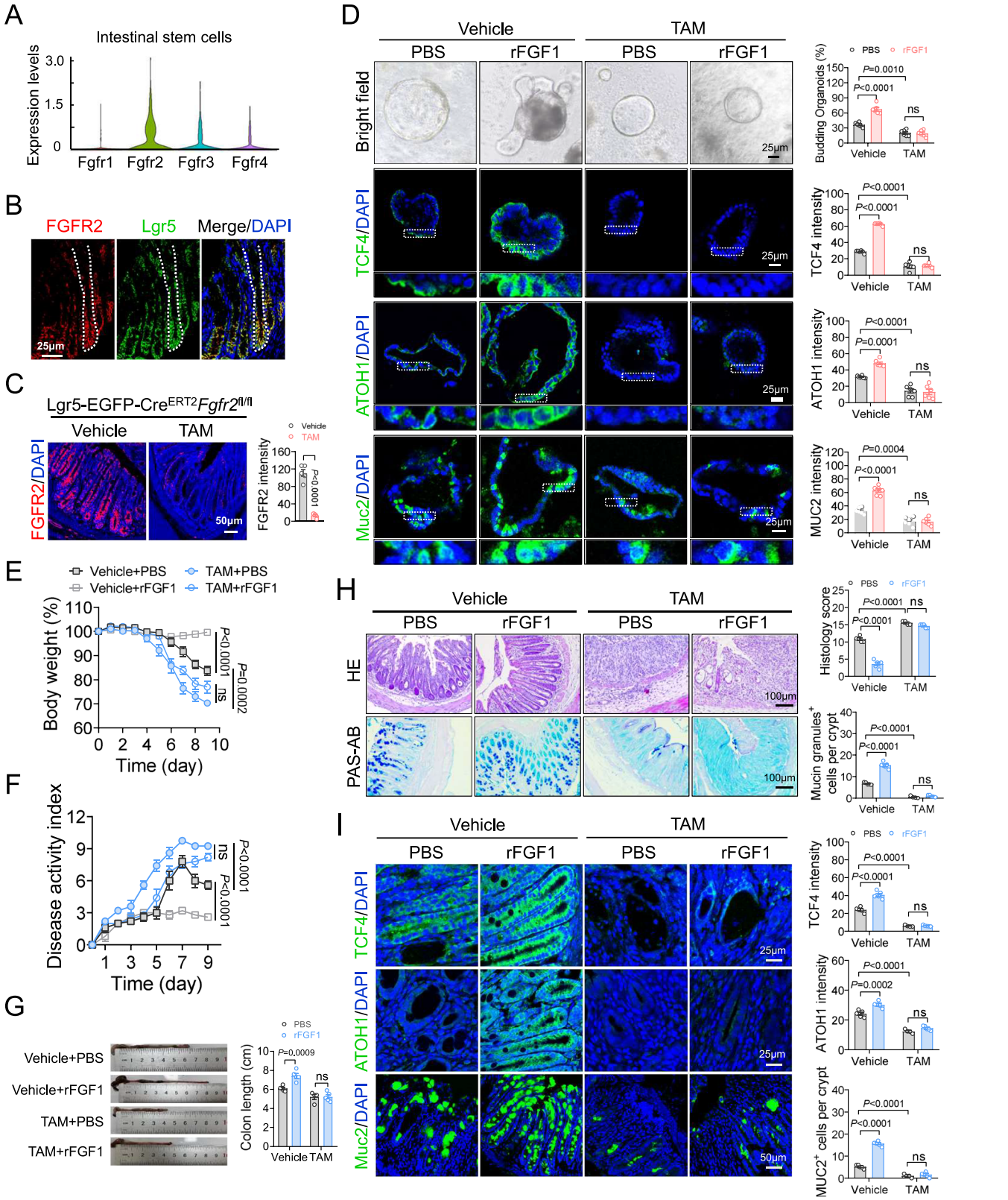

effects of FGF1. These are key issues that need to be addressed in the development of FGF1-based biologics for the treatment of IBD.

In summary, we identified paracrine FGF1 as an epithelial niche-derived cytokine that can precisely drive ISCs to differentiate into goblet cells, providing mechanistic insights into the pathogenesis of IBD and potential therapeutic strategies for IBD treatment. Notably, the regulatory effect of FGF1 on the directional differentiation of goblet cells is independently of proliferation activity, making it a target with great translational prospects.

Methods

Animals and animal welfare

8-week-old male C57BL/6J mice and BALB/c mice were from Beijing Vital River Laboratory Animal Technology Co., Ltd. (Beijing, China).

Fig. 7 | FGFR2 mediates the protective effects of rFGF1 on IBD in mice. A Single-cell RNA sequencing analysis (GSM4983265) showed that *Fgfr2* is highly expressed in stem cells. **B** Representative image of colon distal stained with Lgr5 (green), FGFR2 (red) and DAPI (blue) from the C57BL/6 J mice ($n = 3$). **C** Deletion of *Fgfr2* in Lgr5-EGFP-Cre^{ERT2}*Fgfr2*$^{fl/fl}$ mice treated with vehicle or tamoxifen was confirmed by IF staining ($n = 5$). **D** Murine colonic organoids derived from vehicle or tamoxifen-treated Lgr5-EGFP-Cre^{ERT2}*Fgfr2*$^{fl/fl}$ mice were stimulated with vehicle or rFGF1. Representative images, IF staining of TCF4, ATOH1 and Muc2 in colonic organoids were shown (n = 6). **E**–**I** Vehicle or tamoxifen-treated Lgr5-EGFP-Cre^{ERT2}*Fgfr2*$^{fl/fl}$ mice were challenged with drinking water containing 2.5% DSS to induce UC, followed by colon tissues were harvested and examined (n = 4 for TAM + PBS group, $n = 5$ for other groups). Weight loss (**E**), disease activity index (**F**) and colon length (**G**) of different groups were monitored. **H** H&E staining of distal colon sections and histology scores (upper panel), PAS-AB staining of distal colon sections and mucin granules-positive cells per crypt (lower panel). **I** IF staining of TCF4 (upper panel), ATOH1 (middle panel) and Muc2 (lower panel) in distal colon sections, and its semi-quantification of IF intensity. Data was presented as mean ± SEM. (right panel of **C**) two-tailed unpaired *t*-test; (right panel of **D**–**F**, right panel of **G**–**I**) ordinary two-way ANOVA, followed by Sidak. ns, no significance.

Fgf1$^{fl/fl}$ (S-CKO-02396), *Atoh1*$^{fl/fl}$ (S-CKO-01332), *Fgfr2*$^{fl/fl}$ (S-CKO-02415), VillinCre (C001243), VillinCre^{ERT2} (C001433) and Lgr5-EGFP-Cre^{ERT2} (C001315) mice on C57BL/6 J background were purchased from Cyagen Biosciences (Suzhou) Inc. (Jiangsu, China). Mice with an intestinal epithelial-specific deletion of *Fgf1* (VillinCre*Fgf1*$^{fl/fl}$) and *Atoh1* (VillinCre^{ERT2}*Atoh1*$^{fl/fl}$) mice were generated by crossing VillinCre or VillinCre^{ERT2} animals with mice harboring loxP-flanked *Fgf1* (*Fgf1*$^{fl/fl}$) and *Atoh1* (*Atoh1*$^{fl/fl}$). Lgr5^{+} intestinal epithelial-specific deletion of *Fgfr2* mice (Lgr5-EGFP-Cre^{ERT2}*Fgfr2*$^{fl/fl}$) were generated by crossing Lgr5-EGFP-Cre^{ERT2} recombinase transgenic mice with *Fgfr2*$^{fl/fl}$. Animals were housed in a specific pathogen-free (SPF) animal facility with a controlled environment (22 ± 1 °C, 50–60% humidity, 12-h light/dark cycle, lights on at 7 am) and free access to food and water. All animal procedures conducted in this study were approved by the Animal Care and Use Committee of Wenzhou Medical University, under approval number wydw2022-0202.

Human colon samples

Colonic biopsy samples were obtained from patients (aged 16 to 66 years old) who were newly diagnosed with UC or CD during undergoing clinically indicated endoscopic screening, with controls being tissues from normal sites during biopsy, at the First Affiliated Hospital of Wenzhou Medical University (Zhejiang, China) with written informed consent. These patients did not receive immunotherapy or other drug treatment to avoid the effect of drug treatment on the cytokine levels we observed. Sampling procedures were approved by the ethics committee of the First Affiliated Hospital of Wenzhou Medical University (the approval number is KY2022-R171) and conducted in accordance with the Declaration of Helsinki on ethical principles for medical research involving human subjects. Biopsy samples were immediately fixed in 10% formalin and embedded in paraffin for tissue analysis. The details of human patient information are listed in Supplemental Table 1-2.

Expression and purification of recombinant FGF1

Recombinant matured wild type human FGF1 (mFGF1) and engineered non-mitogenic FGF1 analog FGF1$^{\Delta HBS}$ (rFGF1) were expressed in *E. coli* and purified as described in the previous report[38]. Briefly, the expression of FGF1 was induced by isopropyl-β-D-1-thiogalactopyranoside (IPTG). The cells were harvested and dissolved by sonication in an ice bath. Recombinant mFGF1 was purified by heparin-affinity chromatograph and size exclusion chromatography. RFGF1 were purified using cation exchange column (Source S, GE Healthcare) and size exclusion chromatography. The purity of all above proteins was estimated to be >98% based on SDS-PAGE analysis. The concentration was evaluated using a NanoDrop.

Induction of colitis, treatment and disease score

DSS-induced colitis was performed as previously described in ref. 39. 8-week old male C57BL/6 J, Lgr5-EGFP-Cre^{ERT2}*Fgfr2*$^{fl/fl}$, VillinCre*Fgf1*$^{fl/fl}$ or VillinCre^{ERT2}*Atoh1*$^{fl/fl}$ mice with similar weights were selected and treated with 2.5% DSS (160110, MP Biomedicals) in drinking water for 7 days, then followed with regular water for another 4 days. The mice were intraperitoneally (i.p.) injected with mFGF1 or rFGF1 (0.2 mg/kg) on the 3rd day after 2.5% DSS treatment, until the end of this experiment. Mice were sacrificed for tissue analyses on days 11. TNBS-induced colitis models were established using a method adapted from a published procedure[40]. 8-week old male BALB/c or VillinCre*Fgf1*$^{fl/fl}$ mice with similar weights were anesthetized by isoflurane inhalation, and then 5% (wt/vol) 2,4,6-trinitrobenzenesulfonic acid (TNBS) (P2297, Sigma) in ethanol was rectally administered. To ensure TNBS retention, mice were maintained in a vertical position for 2 min. The mice were intraperitoneally injected with recombinant FGF1 (0.2 mg/kg). Mice were sacrificed for tissue analyses on days 4.

The body weight loss score (body weight loss: 0, ≤0; 1, 0 ~ 5%; 2, 5% ~ 10%; 3, 10% ~ 20%; 4, >20%), bleeding score (intestinal bleeding status: 0, occult blood test negative; 1, occult blood test positive; 2, gross blood stool; 3, colonic hemorrhage) and stool consistency score (fecal shapes: 0, normal; 1, soft stool; 2, viscous stool; 3, liquid stool) of each mouse were tested, recorded and quantified. Disease activity index (DAI) is the sum of body weight loss scores, bleeding scores and stool consistency scores.

Culture and stimulation of murine and human colonic organoids

The culture of murine colonic organoids was performed as previously described in ref. 41. Briefly, crypts extracted from mouse colon tissues were pelleted and re-suspend in Matrigel Matrix (356234, Corning). 50 µl of crypt suspension were distributed to 24-well plates. After the polymerization of Matrigel at 37°C, 5% CO2 for 10 min, the matrix was overlaid with 750 µl of IntestiCult™ Organoid Growth Medium (6005, Stemcell). Organoids treated with vehicle or rFGF1 (500 ng/ml) were harvested and analyzed on day 7.

Human organoids were cultured as described previously[42]. To generate organoids, human colon biopsy samples were cut into 1 mm pieces and washed with cold PBS containing 1% penicillin/streptomycin by pipetting 8-10 times. Samples were treated with Gentle Cell Dissociation Reagent (#100-0485, Stemcell) at 37 °C for 30 min. Pelleted crypts were re-suspend in Matrigel Matrix (356234, Corning) and cultured with human IntestiCult™ Organoid Growth Medium (06010, Stemcell). Organoids treated with vehicle or rFGF1 (500 ng/ml) were harvested and analyzed on day 7.

Adenovirus transfection

Adenovirus was used to deliver short hairpin RNA (shRNA) into organoids to knockdown the expression of *Atoh1*. The knockdown and control virus were produced by WZ Biosciences Inc (Shandong, China). Sequence of shRNA targeting *Atoh1* was constructed into one vector, and the sequence was provided in Supplemental Table 3. Scramble sequence of equal length was constructed in the same vector as control. For cell transfection, murine crypts were incubated with adenovirus at a MOI (multiplicity of infection) of 1000 in IntestiCult™ Organoid Growth Medium (6005, Stemcell) for 30 min and then used to form organoids as described above. The knockdown or over-expressing efficiency was determined by immunofluorescence assay.

Histopathology

5 µm paraffin embedded tissue sections were deparaffinized and rehydrated using xylene and a descending ethanol gradient (100%, 95% and 80%). For PAS-AB staining, alcian blue solution (pH 2.5) was added

to slides for 20 minutes to stain the cells. Slides were washed with PBS for 5 min three times. Periodic acid solution was applied for 5 min. Slides were washed with washed with PBS. Schiff reagent was added to slides for 20 min to stain the cell nucleus. Slides were rinsed in running tap water for 10 min, and then dehydrated with an ascending ethanol gradient (95% and 100%). Slides were mounted and images were acquired by a light microscope (Nikon eclipse Ni, Tokyo, Japan). In statistical analysis, a single value represents the average number of mucin granules^{+} cells from each mouse's five crypts. For hematoxylin & eosin (H&E) staining, hematoxylin was added to slides for 3 min and washed in water. The slides were immersed in PBS for 10 min. Tissues were stained with eosin for 30 s. Slides were transferred to Xylene for 10 min. Slides were mounted and images were acquired by a light microscope (Nikon eclipse Ni, Tokyo, Japan).

Transcriptome sequencing

Total RNA from colon tissues of PBS or rFGF1-treated UC mice was collected using RNAiso Plus and subjected to genome-wide transcriptomic analysis by LC-Bio (Hangzhou, China). Genes that are critical for cell lineage commitment are selected and presented as a heat map. Raw sequencing data were submitted to Gene Expression Omnibus (GSE278384).

Immunofluorescence (IF) and Immunohistochemical (IHC) staining

The distal colon was fixed in 4% paraformaldehyde and embedded in paraffin blocks. For IF staining, tissues were rehydrated and treated for antigen unmasking. Sections were incubated for 10 min in hydrogen peroxide, washed with 0.01 M PBS. Then, tissue sections were blocked in PBS containing 5% bovine serum albumin for 30 minutes at 37°C followed by incubation at 4 °C overnight in PBS containing 1% bovine serum albumin and primary antibodies. For murine colonic organoids, organoids were cultured and fixed with 4% paraformaldehyde for 30 min. Organoids were then incubated at 4 °C overnight with 30% sucrose, followed by incubated with O.C.T. Compound for 15 min at −20 °C. After washed three time with PBS, organoids were blocked in PBS containing 5% bovine serum albumin for 30 min at 37 °C followed by incubation at 4 °C overnight in primary antibodies. The primary antibodies are listed below: rabbit anti-FGF1 (1:200, 17400, Proteintech), mouse anti-FGF1 (1:100, sc-55520, Santa Cruz Biotechnology), EpCAM (1:800, CST42515, Cell Signaling Technology), Col1α1 (1:100, CST72026, Cell Signaling Technology), ATOH1 (1:400, 21215-1-AP, Proteintech), TCF4 (1:100, ab217668, Abcam), Muc2 (1:400, ab272692, Abcam), Dclk1 (1:300, CST62257, Cell Signaling Technology), ChgA (1:200, sc-393941, Santa Cruz Biotechnology), Fabp1 (1:50, CST13368, Cell Signaling Technology), Ki67 (1:400, ab15580, Abcam), FGFR2 (1:200, CST23328S, Cell Signaling Technology) and Lgr5 (1:100, UM870104, ORIGENE). After washing the slides with PBS, the sections were incubated with anti-rabbit IgG Fab2 Alexa Fluor® 488 (1:400, ab150073, Abcam), anti-mouse IgG Fab2 Alexa Fluor® 647 (1:400, ab150105, Abcam) and anti-mouse IgG Fab2 Alexa Fluor® 488 (1:400, ab150105, Abcam). Nuclei were counterstained with DAPI. Fluorescent images were captured with a Nikon C2si Confocal Microscope.

For IHC staining, tissues were rehydrated and treated for antigen unmasking. Then colon sections were permeabilized in PBS with 0.2% Triton X-100 for 15 min at room temperature, then blocked with PBS containing 0.5% bovine serum albumin. After 1 h, the sections were incubated with primary antibodies at 4 °C overnight: Ki67 (1:400, ab15580, Abcam). And then incubated with a biotinylated secondary antibody of anti-rabbit IgG at room temperature for 1 h. Next, the colon sections were treated with Diaminobenzidine (DAB) Histochemistry Kit. Finally, the nuclei were stained with hematoxylin. Images were acquired by a light microscope (Nikon eclipse Ni, Tokyo, Japan). In statistical analysis, a single value represents the average number of Ki67 positive cells in each mouse's five crypts.

Western blots

Protein expression in distal colon was detected by Western blots. Equal amounts of total protein were loaded on and separated by 10% SDS-PAGE and then transferred onto PVDF Membrane (Millipore, Billerica, MA). The membranes were blocked for 1 h in TBST-buffered saline containing 5% bovine serum albumin (BSA) (w/v) and incubated with primary antibodies, including FGF1(1:1000, 17400, Proteintech), cleaved NICD (1:1000, CST4147S, Cell Signaling Technology), β-catenin (1:1000, CST8480, Cell Signaling Technology), Axin2 (1:1000, 20540-1-AP, Proteintech), p-ERK1/2 (1:1000, CST4370S, Cell Signaling Technology), ERK1/2 (1:1000, CST9102S, Cell Signaling Technology), GAPDH (1:1000, CST2118S, Cell Signaling Technology), overnight at 4 °C, followed by incubation for 1 h with appropriate secondary antibodies. Protein bands were detected with a Chemiluminescence Detection Kit for HRP (2148903, Biological Industries) and developed using a chemiDoc XRS+ (Bio-Rad). Densitometer analysis was performed using the Image J analysis program.

RNA Isolation and Real-Time quantitative PCR

Total RNA was extracted from the indicated cells or mouse colon tissues with TRIzol reagent (TransGen Biotech) according to the manufacturer's instructions. RNA samples were reverse-transcribed into cDNA with a PrimeScript RT Reagent kit (TransGen Biotech). The cDNA samples were amplified by real-time PCR with a SYBR Premix Ex Taq kit (Vazyme Biotech) on a Roche LightCycler 480 II (Roche). The expression of target genes was normalized to expression of housekeeping gene β-Actin. The primers used were listed in Supplemental Table 3.

Luciferase reporter analysis

HT-29 cell lines were purchased from National Collection of Authenticated Cell Cultures, which were cultured under conventional conditions of 37 °C and 5% CO_2. Take HT29 cells in logarithmic growth phase and inoculate 1.5×10^5 cells per well into a 24 well plate, with a total volume of 300 μL per well. After plating 24 hours, HT-29 cells were transfected with Lipo3000 (Gibco) using 500 ng pcDNA3.1 or pcDNA3.1-TCF4 along with 750 ng pGL3-Basic, pGL3-*Atoh1* promoter luc or pGL3-Atoh1 promoter-MUT luc. After 48 h the culture medium was removed and luciferase activity was measured by Dual-Glo Luciferase Assay System (E1910, Promega) according to the manufacturer's instructions. Firefly luciferase activity was normalized to the renilla luciferase activity.

Chromatin immunoprecipitation-qRCR (ChIP-qRCR) assay

The ChIP assay was performed using the SimpleChIP Plus Enzymatic Chromatin IP Kit (Cell Signaling Technology, 9004) according to the manufacturer's instructions. Briefly, colon tissues were homogenized, crosslinked with 1.5% formaldehyde, and treated with a protease inhibitor cocktail (PIC) for 20 min at room temperature. Crosslinking was quenched with glycine solution for 5 min. The resulting pellet was collected by centrifugation and resuspended with PBS containing 0.5% PIC. Then using a Dounce homogenizer to obtain a single cell suspension. Collecting cell pellet by centrifugation and resuspended in nuclear lysis buffer containing Micrococcal Nuclease and incubated at 37 °C for 20 min. The chromatin fragments were immunoprecipitated overnight at 4 °C with TCF4 (1:100, ab217668, Abcam) or normal IgG antibody as a control. The chromatin-antibody complex was subsequently incubated with ChIP-Grade Protein G Agarose Beads for 2 hours at 4 °C. The chromatin was eluted from the ChIP elution buffer, and the results were quantified using qRT-PCR assay.

TUNEL staining

The colon sections were stained with DeadEnd™ Fluorometric TUNEL System (Promega, G3250) according to the manufacturer's protocol. DAPI was used for nuclei staining. Images were visualized and captured with a confocal laser scanning microscope (Nikon). The number of

nucleus and TUNEL-positive cells per field was counted, and the percentage of TUNEL-positive cells was calculated. In statistical analysis, a single value represents the average percentage of TUNEL-positive cells in each mouse's two fields.

Statistical analysis

Variable representative images were obtained from each stained section, and positivity of all markers was manually or automatically quantitated using Image J software. Quantitative data were expressed as mean ± SEM. Statistical analysis of data was performed using GraphPad Prism. The Shapiro-Wilk test was used to test the normality of data distribution. If P value > 0.05, parametric statistical tests were used. If P value < 0.05, non-parametric statistical methods (Mann-Whitney test for unpaired t-test, Kruskal-Wallis for one-way) were used and indicated in the related legends. For the comparison of two groups, an unpaired t-test was used. One or two-way ANOVA was used for multiple groups. A P value < 0.05 was considered statistically significant.

Reporting summary

Further information on research design is available in the Nature Portfolio Reporting Summary linked to this article.

Data availability

The RNA-seq data generated in this study have been deposited in the GEO database under accession code GSE278384. All data are included in the Supplementary Information or available from the authors. Source data are provided with this paper.

References

1. Berre, C. L., Honap, S. & Peyrin-Biroulet, L. Ulcerative colitis. *Lancet* **402**, 571–584 (2023).
2. Torres, J., Mehandru, S., Colombel, J. F. & Peyrin-Biroulet, L. Crohn's disease. *Lancet* **389**, 1741–1755 (2017).
3. Ng, S. C. et al. Worldwide incidence and prevalence of inflammatory bowel disease in the 21st century: a systematic review of population-based studies. *Lancet* **390**, 2769–2778 (2017).
4. Gros, B. & Kaplan, G. G. Ulcerative Colitis in Adults: A Review. *JAMA* **330**, 951–965 (2023).
5. Chang, J. T. Pathophysiology of Inflammatory Bowel Diseases. *N. Engl. J. Med* **383**, 2652–2664 (2020).
6. Beumer, J. & Clevers, H. Cell fate specification and differentiation in the adult mammalian intestine. *Nat. Rev. Mol. Cell Biol.* **22**, 39–53 (2021).
7. Parikh, K. et al. Colonic epithelial cell diversity in health and inflammatory bowel disease. *Nature* **567**, 49–55 (2019).
8. Peterson, L. W. & Artis, D. Intestinal epithelial cells: regulators of barrier function and immune homeostasis. *Nat. Rev. Immunol.* **14**, 141–153 (2014).
9. Okumura, R. & Takeda, K. Maintenance of intestinal homeostasis by mucosal barriers. *Inflamm. Regen.* **38**, 5 (2018).
10. Gustafsson, J. K. & Johansson, M. E. V. The role of goblet cells and mucus in intestinal homeostasis. *Nat. Rev. Gastroenterol. Hepatol.* **19**, 785–803 (2022).
11. Kang, Y., Park, H., Choe, B. H. & Kang, B. The Role and Function of Mucins and Its Relationship to Inflammatory Bowel Disease. *Front Med (Lausanne)* **9**, 848344 (2022).
12. Kayama, H., Okumura, R. & Takeda, K. Interaction Between the Microbiota, Epithelia, and Immune Cells in the Intestine. *Annu Rev. Immunol.* **38**, 23–48 (2020).
13. Gehart, H. & Clevers, H. Tales from the crypt: new insights into intestinal stem cells. *Nat. Rev. Gastroenterol. Hepatol.* **16**, 19–34 (2019).
14. Alvarado, D. M. et al. Epithelial Indoleamine 2,3-Dioxygenase 1 Modulates Aryl Hydrocarbon Receptor and Notch Signaling to Increase Differentiation of Secretory Cells and Alter Mucus-Associated Microbiota. *Gastroenterology* **157**, 1093–1108.e1011 (2019).
15. Schumacher, M. A. et al. Sprouty2 limits intestinal tuft and goblet cell numbers through GSK3beta-mediated restriction of epithelial IL-33. *Nat. Commun.* **12**, 836 (2021).
16. Lin, X. et al. IL-17RA-signaling in Lgr5(+) intestinal stem cells induces expression of transcription factor ATOH1 to promote secretory cell lineage commitment. *Immunity* **55**, 237–253.e238 (2022).
17. Beenken, A. & Mohammadi, M. The FGF family: biology, pathophysiology and therapy. *Nat. Rev. Drug Discov.* **8**, 235–253 (2009).
18. Gasser, E., Sancar, G., Downes, M. & Evans, R. M. Metabolic Messengers: fibroblast growth factor 1. *Nat. Metab.* **4**, 663–671 (2022).
19. Matsuura, M. et al. Therapeutic effects of rectal administration of basic fibroblast growth factor on experimental murine colitis. *Gastroenterology* **128**, 975–986 (2005).
20. Zeeh, J. M. et al. Keratinocyte growth factor ameliorates mucosal injury in an experimental model of colitis in rats. *Gastroenterology* **110**, 1077–1083 (1996).
21. Sandborn, W. J. et al. Repifermin (keratinocyte growth factor-2) for the treatment of active ulcerative colitis: a randomized, double-blind, placebo-controlled, dose-escalation trial. *Aliment Pharm. Ther.* **17**, 1355–1364 (2003).
22. Yang, Q., Bermingham, N. A., Finegold, M. J. & Zoghbi, H. Y. Requirement of Math1 for secretory cell lineage commitment in the mouse intestine. *Science* **294**, 2155–2158 (2001).
23. Shroyer, N. F. et al. Intestine-specific ablation of mouse atonal homolog 1 (Math1) reveals a role in cellular homeostasis. *Gastroenterology* **132**, 2478–2488 (2007).
24. Lo, Y. H. et al. Transcriptional Regulation by ATOH1 and its Target SPDEF in the Intestine. *Cell Mol. Gastroenterol. Hepatol.* **3**, 51–71 (2017).
25. Gregorieff, A. et al. The ets-domain transcription factor Spdef promotes maturation of goblet and paneth cells in the intestinal epithelium. *Gastroenterology* **137**, 1333–1345.e1331-1333 (2009).
26. Shroyer, N. F., Wallis, D., Venken, K. J., Bellen, H. J. & Zoghbi, H. Y. Gfi1 functions downstream of Math1 to control intestinal secretory cell subtype allocation and differentiation. *Genes Dev.* **19**, 2412–2417 (2005).
27. Artavanis-Tsakonas, S., Rand, M. D. & Lake, R. J. Notch signaling: cell fate control and signal integration in development. *Science* **284**, 770–776 (1999).
28. Baulies, A. et al. The Transcription Co-Repressors MTG8 and MTG16 Regulate Exit of Intestinal Stem Cells From Their Niche and Differentiation Into Enterocyte vs Secretory Lineages. *Gastroenterology* **159**, 1328–1341.e1323 (2020).
29. Zhang, X. et al. Receptor specificity of the fibroblast growth factor family. The complete mammalian FGF family. *J. Biol. Chem.* **281**, 15694–15700 (2006).
30. Xie, Y. et al. FGF/FGFR signaling in health and disease. *Signal Transduct. Target Ther.* **5**, 181 (2020).
31. Zinkle A. & Mohammadi, M. A threshold model for receptor tyrosine kinase signaling specificity and cell fate determination. *F1000Res.* **7**, 872 (2018).
32. Beaudry, K. et al. Dual-specificity phosphatase 6 deletion protects the colonic epithelium against inflammation and promotes both proliferation and tumorigenesis. *J. Cell Physiol.* **234**, 6731–6745 (2019).
33. Bankaitis, E. D., Ha, A., Kuo, C. J. & Magness, S. T. Reserve Stem Cells in Intestinal Homeostasis and Injury. *Gastroenterology* **155**, 1348–1361 (2018).
34. Barker, N. Adult intestinal stem cells: critical drivers of epithelial homeostasis and regeneration. *Nat. Rev. Mol. Cell Biol.* **15**, 19–33 (2014).
35. Pitsouli, C., Apidianakis, Y. & Perrimon, N. Homeostasis in infected epithelia: stem cells take the lead. *Cell Host Microbe* **6**, 301–307 (2009).

36. He, X. C. et al. BMP signaling inhibits intestinal stem cell self-renewal through suppression of Wnt-beta-catenin signaling. *Nat. Genet* **36**, 1117–1121 (2004).
37. Castillo-Azofeifa, D. et al. Atoh1(+) secretory progenitors possess renewal capacity independent of Lgr5(+) cells during colonic regeneration. *EMBO J.* **38**, e99984 (2019).
38. Huang, Z. et al. Uncoupling the Mitogenic and Metabolic Functions of FGF1 by Tuning FGF1-FGF Receptor Dimer Stability. *Cell Rep.* **20**, 1717–1728 (2017).
39. Bulek, K. et al. Epithelial-derived gasdermin D mediates nonlytic IL-1beta release during experimental colitis. *J. Clin. Invest* **130**, 4218–4234 (2020).
40. Tan, G., Huang, C., Chen, J., Chen, B. & Zhi, F. Gasdermin-E-mediated pyroptosis participates in the pathogenesis of Crohn's disease by promoting intestinal inflammation. *Cell Rep.* **35**, 109265 (2021).
41. Zhou, Q. et al. Catechol-O-Methyltransferase Loss Drives Cell-Specific Nociceptive Signaling via the Enteric Catechol-O-Methyltransferase/microRNA-155/Tumor Necrosis Factor alpha Axis. *Gastroenterology* **164**, 630–641.e634 (2023).
42. Matsuzawa-Ishimoto, Y. et al. An intestinal organoid-based platform that recreates susceptibility to T-cell-mediated tissue injury. *Blood* **135**, 2388–2401 (2020).

Acknowledgements

This work was supported by grants from the Natural Science Foundation of China (82273996 to J.N.), the Natural Science Foundation of Zhejiang Province (LZYQ25H310001 to J.N.), the Pharmaceutics Summit Advancement Disciplines of Zhejiang Province to X.L.

Author contributions

J.L.N., X.K.L., Z.F.H. conceived the project and designed experiments. Q.L., S.D.Z., J.R.Z., Y.J., T.L.C., R.Y.L., J.X.L., W.J.X., T.Z.W., S.Y.T., L.Y., X.K.L., Z.F.H., J.L.N. performed experiments, analyzed data and participated in discussion of the results. Y.J. provided clinical samples. Q.L., L.Y., Z.F.H., J.L.N. wrote this manuscript.

Competing interests

The authors declare no competing interests.

Additional information

Supplementary information The online version contains supplementary material available at https://doi.org/10.1038/s41467-025-58644-2.

Correspondence and requests for materials should be addressed to Zhifeng Huang or Jianlou Niu.

Peer review information *Nature Communications* thanks David Alvarado, and the other, anonymous, reviewer(s) for their contribution to the peer review of this work. A peer review file is available."